

ARTHUR LAKES LIBRARY
COLORADO SCHOOL of MINES
GOLDEN, COLORADO 80401

Adsorption of Sulfur Dioxide
on Spent Shale in Packed Beds

by
Muhammad A. Hasanain

ProQuest Number: 10782148

All rights reserved

INFORMATION TO ALL USERS

The quality of this reproduction is dependent upon the quality of the copy submitted.

In the unlikely event that the author did not send a complete manuscript and there are missing pages, these will be noted. Also, if material had to be removed, a note will indicate the deletion.



ProQuest 10782148

Published by ProQuest LLC (2018). Copyright of the Dissertation is held by the Author.

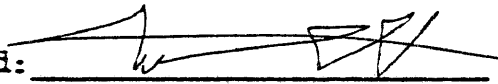
All rights reserved.

This work is protected against unauthorized copying under Title 17, United States Code
Microform Edition © ProQuest LLC.

ProQuest LLC.
789 East Eisenhower Parkway
P.O. Box 1346
Ann Arbor, MI 48106 – 1346

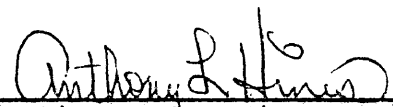
ARTHUR LAKES LIBRARY
COLORADO SCHOOL of MINES
GOLDEN, COLORADO 80401

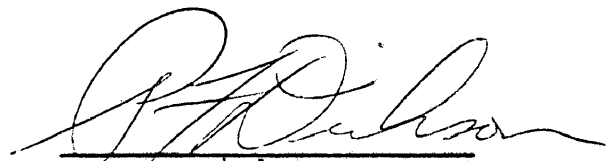
A Thesis submitted to the Faculty and the Board of Trustees of the Colorado School of Mines in partial fulfillment of the requirements for the degree of Master of Science (Chemical and Petroleum-Refining Engineering).

signed: 
Muhammad A. Hasanain

Golden, Colorado

Date: Dec. 5th, 1977

approved: 
Anthony A. Hines
Thesis Advisor


P. F. Dickson
Head of Department

Golden, Colorado

Date: Dec. 5th, 1977

ARTHUR EAKES LIBRARY
COLORADO SCHOOL of MINES
GOLDEN, COLORADO 80401

THANK GOD

ABSTRACT

This investigation was undertaken in order to study the adsorption of sulfur dioxide on spent shale which was retorted for two hours and at a temperature of 700°C. An apparatus for oil shale retorting and the adsorption study was designed and constructed. The adsorbent was selected from samples of spent shale which were retorted at temperatures ranging from 300°C to 1000°C for retorting periods of 2 hours, 5 hours, and 15 hours. The primary objectives were to determine the effects of retorting temperature and time on the adsorption properties of spent shale. Adsorption studies were conducted on the material which was retorted for two hours. Sulfur dioxide concentrations considered were 993, 1999, 2999, 4998, 7226, and 9704 PPM SO₂ in N₂; and adsorption temperatures were 10°C, 27°C, and 40°C. The experimental breakthrough curves were fitted to theoretical plots derived by Antonson () using an intraparticle diffusion model. From the curve fits of breakthrough curves, intraparticle diffusivities were calculated at two different temperatures. The equilibrium isotherms were fitted to Langmuir, Freundlich and Polanyi and Dubinin types of equilibrium isotherms. The heat of adsorption was estimated at a loading of $3.5 \times 10^{-3} \frac{\text{gm SO}_2}{\text{cm}^3 \text{solid}}$. It was found to equal 4.918 Kcal/mole. Finally the activation energy was estimated from the Arrhenius plots for three different concentrations.

TABLE OF CONTENTS

	Page
ABSTRACT	iii
LIST OF FIGURES	v
LIST OF TABLES	vii
ACKNOWLEDGMENTS	viii
INTRODUCTION	1
THEORY	5
Equilibrium Isotherms	5
Heat of Adsorption	9
Mass Transfer Mechanisms	10
EQUIPMENT AND PROCEDURE	14
Adsorbent preparation	14
Adsorption equipment	16
Experimental procedure	19
RESULTS AND DISCUSSION	20
Sample selection	20
Effect temperature & concentration on breakthrough curves	32
Equilibrium isotherms	32
Heat of adsorption	55
Intraparticle diffusion coefficients	55
Activation energy	69
CONCLUSION AND RECOMMENDATIONS	71
NOMENCLATURE	73
LIST OF REFERENCES	75
APPENDIX "A" - Experimental Data	79
APPENDIX "B" - Sample Calculations	88

LIST OF FIGURES

	Page
1. Schematic of Oil Shale Retort	15
2. Gas Adsorption Apparatus	17
3. BET Surface Area Analysis	28
4. Adsorption of SO ₂ on Different Spent Shale	31
5. Experimental Breakthrough Curves (993, 2999, and 7226 PPM) at 10°C	33
6. Experimental Breakthrough Curves (1999, 4998, and 9704 PPM) at 10°C	34
7. Experimental Breakthrough Curves (993, 2999, and 7226 PPM) at 27°C	35
8. Experimental Breakthrough Curves (1999, 4998, and 9704 PPM) at 27°C	36
9. Experimental Breakthrough Curves (993, 2999, and 7226 PPM) at 40°C	37
10. Experimental Breakthrough Curves (1999, 4998, and 9704 PPM) at 40°C	38
11. Experimental Breakthrough Curves (10, 27, and 40°C) for 1999 PPM	39
12. Least Square Fit to Langmuir Model (T=10°C)	41
13. Least Square Fit to Langmuir Model (T=27°C)	42
14. Least Square Fit to Langmuir Model (T=40°C)	43
15. Equilibrium Data Fit to Langmuir Model	45
16. Least Square Fit for Freundlich Model at 10°C	46
17. Least Square Fit for Freundlich Model at 27°C	47
18. Least Square Fit for Freundlich Model at 40°C	48
19. Equilibrium Data Fit to Freundlich Model	50

20.	Least Square Fit for Dubinin Model at 10°C	51
21.	Least Square Fit for Dubinin Model at 27°C	52
22.	Least Square Fit for Dubinin Model at 40°C	53
23.	Polanyi Model	47
24.	Equilibrium Isosters	58
25.	Curve Fit for 993 PPM at 10°C	61
26.	Curve Fit for 2999 PPM at 10°C	62
27.	Curve Fit for 4998 PPM at 10°C	63
28.	Curve Fit for 993 PPM at 40°C	64
29.	Curve Fit for 1999 PPM at 40°C	65
30.	Curve Fit for 4998 PPM at 40°C	66
31.	Diffusion Coefficient as a Function of Concentration at 10°C	67
32.	Diffusion Coefficient as a Function of Concentration at 40°C	68
33.	Arrhenius Plot	70

LIST OF TABLES

	Page
I. Chemical Analysis of Oil Shale Retorted for 2 Hours	21
II. Chemical Analysis of Oil Shale Retorted for 5 Hours	22
III. Chemical Analysis of Oil Shale Retorted for 15 Hours	23
IV. X-Ray Analysis of Oil Shale Retorted for 2 Hours	24
V. X-Ray Analysis of Oil Shale Retorted for 5 Hours	25
VI. X-Ray Analysis of Oil Shale Retorted for 15 Hours	26
VII. BET Surface Area Analysis	27
VIII. Adsorption of SO ₂ on Different Samples of Spent Shale	30
IX. Equilibrium Data and Langmuir Constants	44
XX. Equilibrium Data and Freundlich Constants	49
XI. Equilibrium Data and Dubinin Constants	54
XII. Equilibrium Data to Fit Polanyi Model	56
XIII. Diffusion Coefficients	60

Acknowledgments

The author wishes to express his gratitude to Dr. Anthony L. Hines for his guidance in all aspects of this work. Appreciation is also extended to Dr. R. Baldwin and Dr. E. Sloan for acting as committee members. Acknowledgments also go to Dr. John J. Duvall, Mr. Howard Jensen, and Dr. Richard E. Poulson of the Laramie Energy Research Center for their support throughout the project. Also the support of the United States Energy Research and Development Administration under contract number E(29-2)-3780 is gratefully acknowledged. And last, but not least, the author wishes to gratefully acknowledge his wife, Zaheiah, for her patience and good humor in the face of occasional adversity.

INTRODUCTION

There are two major processes used to produce oil from oil shale. One of the major processes is mining the shale and recovering the oil in an above-ground retorting facility. The other process is removing the oil from an underground formation in an in situ process.

Above ground retorting processes, although studied extensively, suffer from a number of ecological problems associated with the disposal of large quantities of spent shale. It has been estimated that the production of 250,000 barrels per day of shale oil will create more than 100 million tons of spent shale annually. Using the TOSCO II process and retorting 35 gal/ton shale, in which the spent shale was 81 weight percent of the original unretorted shale, Striffler, Wymore and Berg (33) estimated that the spent shale from a 250,000 barrel/day industry would cover an area of more than 44,000 acre feet annually.

The in situ approach, however, is perhaps the more attractive of the two major processes since the oil is extracted from the shale by heating the underground formation. This process eliminates mining the shale and the pollution problem that accompanies the disposal of spent shale.

In situ processing of oil shale is mainly based on the initiation of combustion or introduction of heat into the formation which results in the decomposition of kerogen into

bitumen, that is converted to oil, residual carbon, hydrocarbon gases, and combustion products. The relatively lower viscosity oil, combustion gases, hydrocarbon vapors, and water produced during the process then flows horizontally through induced fractures and through the shale structure to surrounding wells where they are collected. The rate at which the burn front moves through the formation depends on a number of factors, including shale porosity, diffusivity, permeability, oil content, and the rate of air injection.

For a sizeable shale oil reserve to be recovered, several fundamental questions must be answered, common to both in situ and above ground retorting processes. One of these questions is the adsorptive and absorptive properties of the spent shale and the transfer rates of gases flowing through the formation. It has been estimated (12) that for a 50,000 barrel/day in situ process with no gas recirculation and with all the exhaust gas flared and vented to the atmosphere that 70,714 tons per year of sulfur dioxide would be emitted. Assuming 75% gas recirculation and cleaning the remaining 25% to a sulfur dioxide level of 500 PPM, the Colorado emission standard, 8406 tons per year of SO_2 would still be emitted to the atmosphere. Recently it was noted that less SO_2 than was expected was given off from the controlled state retort at Laramie and this was attributed to the uptake of SO_2 by the oil shale.

In this work the adsorption of SO_2 on spent shale was investigated. Breakthrough curves and equilibrium isotherms were obtained at three different temperatures and heat of

adsorption and diffusion coefficients were calculated. Spent shale samples were produced by retorting raw shale which was obtained from Laramie, Wyoming. The particular material used contained 35 gallons of oil per ton of shale as found by Fischer Assay.

In one investigation, spent shale samples from both above and below the Mahogany Marker were analyzed by Culberston, Nevens, and Hillingshead (7) and samples from both zones contained more than 9% total residual carbon and large percentages of calcium, magnesium, and iron oxides. At retorting temperatures in the presence of water, the carbon that remains in the shale should be activated to some extent and should provide an effective adsorbent for hydrocarbon and combustion gases. Upon considering the composition of the spent shale, the uptake of gases formed during retorting is quite plausible.

The removal of sulfur dioxide from a gas stream can be carried out by several different processes. For example, the "chemico-basic" process uses a slurry of MgO to react with SO₂ to form magnesium sulfate whereas in the limestone wet scrubbing process calcium sulfate is formed. A third process makes use of sodium salts to react with SO₂ to form sodium sulfite/bisulfite. Another method makes use of the activated carbon that is produced from charred peanut hulls, as demonstrated by Hatfield, Murphy, and Hines (16).

Spent shale from above ground facilities can be used as an adsorbent of SO₂ from the process gas streams at a low cost

in industry. Also, the introduction of combustion gases into the underground formation where in situ processing has occurred appears to be an effective method for disposing of waste gases.

THEORY

In this investigation, there are two types of information necessary to describe the unsteady state adsorption behavior resulting from the contact of a fluid containing an adsorbate and a solid adsorbent: 1) equilibrium relation between concentration of adsorbate in gas phase and the concentration of adsorbate within the particle, and 2) the mechanism governing the transfer of adsorbate from one phase to another must be known or estimated.

Equilibrium Isotherms

Equilibrium isotherms, which can be of several types including 1) irreversible, 2) unfavorable, 3) linear and 4) favorable, have been modelled by many theoretical and semi-empirical equations. The equilibrium isotherm equations used in this study are some of the most widely used. They are the Langmuir isotherm model, the Freundlich equation and the Polanyi potential model.

Langmuir Isotherm

The derivation is carried out by using a measure of the concentration of the gas adsorbed on the surface. The following assumptions are used for the derivation:

- 1) All the surface of the solid has the same activity for adsorption.
- 2) There is no interaction between adsorbed molecules.

- 3) All the adsorption occurs by the same mechanism, and each adsorbent complex has the same structure.
- 4) The extent of adsorption is less than one complete monomolecular layer on the surface.

In the system of solid surface and gas, the molecules of gas will be continually striking the surface and a fraction of these will adhere. Introducing the concept of an adsorbent concentration q^* , expressed in moles per gram of solid, and \bar{C}_m which represents the concentration corresponding to a complete monomolecular layer on the solid, then the rate of adsorption, moles/sec-gm solid is:

$$r_a = k_c C^* (\bar{C}_m - q^*) \quad \text{Eq. (1)}$$

where,

$$k_c = \text{forward reaction constant}$$

$$C^* = \text{adsorbate concentration.}$$

The rate of desorption is given by:

$$r_d = k'_c q^* \quad \text{Eq. (2)}$$

where,

$$k'_c = \text{reverse reaction rate constant}$$

at equilibrium, $r_a = r_d$

$$k'_c q^* = k_c C^* (\bar{C}_m - q^*) \quad \text{Eq. (3)}$$

$$\text{or } q^* = \frac{a_1 C^*}{1 + a_2 C^*} \quad \text{Eq. (4)}$$

$$\text{where } a_1 = \frac{k_c}{k'_c} \bar{C}_m,$$

$$\text{and } a_2 = \frac{k_c}{k'_c}.$$

Freundlich Isotherm

This isotherm equation is usually used over a small concentration range, and particularly for dilute solutions. The adsorption isotherms are described by an empirical expression usually attributed to Freundlich.

$$q^* = K[C^*]^{1/n} \quad \text{Eq. (5)}$$

where q^* is the apparent adsorption per unit weight of adsorbent, and K and n are constant. C^* is the adsorbate concentration.

Dubinin-Polanyi Isotherm

Dubinin (9) and his collaborators derived the isotherm equation using the potential theory originally formulated by Polanyi (25). According to Polanyi's treatment, the "adsorption space" in the vicinity of a solid surface is characterized by a series of equipotential surfaces, surfaces of the same adsorption potential. When the volume between the two surfaces of a molecule is filled with adsorbate, the equilibrium pressure is P and the adsorption potential at the surface is obtained directly from the usual expression for chemical potential,

$$\Delta G = \mu_2 - \mu_1 = -RT \ln \frac{P_0}{P} \quad \text{Eq. (6)}$$

where P_0 = saturated pressure of the adsorbate

ΔG = difference in free energy between adsorbed species and the corresponding saturated liquid at the same temperature

μ_2 = chemical potential of sorbed species

μ_1 = chemical potential of saturated liquid

The basic postulate of Polanyi's theory is that, for a given system, the adsorption potential is independent of temperature and depends only on the filled volume of the adsorption space, i.e.,

$$\Delta G = f(W) , \left(\frac{\partial \Delta G}{\partial T} \right)_W = 0 \quad \text{Eq. (7)}$$

The volume W is given by

$$W = \frac{x}{\rho} \quad \text{Eq. (8)}$$

where x = adsorption in grams corresponding to pressure P

ρ = fluid density.

A plot of ΔG vs W yields a "characteristic curve" which is independent of temperature.

Polanyi made no attempt to derive an expression for the adsorption isotherm from the potential theory, but Dubinin (9,10) and his collaborators have developed such an expression. This was done by introducing an affinity coefficient, β , where

$$\beta = \frac{\Delta G_1}{\Delta G_2} \quad \text{Eq. (9)}$$

Dubinin claimed that for two different vapors at the same filling W of the adsorption space on a given solid, the adsorption potentials will bear a constant ratio to one another no matter what the actual value of W.

Now if adsorbate "2" is a vapor taken as an arbitrary standard, then Eq. (9) may be rewritten as,

$$\beta = \frac{\Delta G}{\Delta G_0} \quad \text{Eq. (10)}$$

where the symbols with suffix zero refer to the standard vapor and those without a suffix to the other vapor.

The characteristic curve is defined in an alternative way for the standard vapor as,

$$W = f(\Delta G_0) \quad \text{Eq. (11)}$$

upon inserting Eq. (10), Eq. (11) becomes

$$W = f(\Delta G/\beta) \quad \text{Eq. (12)}$$

Dubinina advanced arguments favoring the view that the volume space may be expressed as a Gaussian function of the adsorption potential. For the standard vapor, this becomes

$$W = W_0 e^{-a' \Delta G_0^2} \quad \text{Eq. (13)}$$

where W_0 = total volume of all micropores

a' = constant characterizing the pore size distribution

By reference to Eq. (10), Eq. (13) can be written as

$$W = W_0 e^{-a' (\Delta G/\beta)^2} \quad \text{Eq. (14)}$$

Substitution for ΔG from Eq. (6), Eq. (14) becomes,

$$W = W_0 \exp\left[-\frac{a'}{\beta^2} (2.303RT \log_{10} \frac{P_0}{P})^2\right] \quad \text{Eq. (15)}$$

or

$$\log_{10} W = \log_{10} W_0 - B \left(\log_{10} \frac{P_0}{P}\right)^2 \quad \text{Eq. (16)}$$

where

$$B = 2.303 \frac{a'}{\beta^2} (RT)^2$$

Heat of adsorption

The equilibrium data also yield values for the heat of adsorption. Hersh (17) has shown that at constant loading

$$\frac{\Delta H_s}{R} = -\left[\frac{\partial (\ln P)}{\partial (1/T)}\right]_{q^*} \quad \text{Eq. (18)}$$

plots of $\ln P$ vs $1/T$ can be analyzed graphically for the slope at constant loading in order to obtain ΔH_s . A typical isoster

and the calculated value of heat of adsorption are described in the results section.

Mass Transfer Mechanisms

A differential material balance for the fluid phase is to be written before considering the transfer of adsorbate from one phase to the next. The appropriate balance is

$$v \frac{\partial C}{\partial Z} + \frac{\partial C}{\partial t} + \frac{1}{m} \frac{\partial \sigma}{\partial t} = D_L \left(\frac{\partial^2 C}{\partial z^2} \right) \quad \text{Eq. (19)}$$

$$m = \frac{\epsilon \rho_L}{\rho_B}, \quad R = \frac{\partial \sigma}{\partial t}$$

ρ_L = bed bulk density

ρ_B = fluid density

ϵ = bed void volume

The last term on the right side of Eq. (19) accounts for axial diffusion. Acrivos (1) has used the equation in this form, although Rosen and most other authors have neglected it based on the assumption that the axial diffusion is small compared to the bulk transfer term ($v \frac{\partial C}{\partial Z}$). Using this assumption, Eq. (19) can be reduced to

$$v \left(\frac{\partial C}{\partial Z} \right) + \left(\frac{\partial C}{\partial t} \right) + \frac{1}{m} \left(\frac{\partial \sigma}{\partial t} \right) = 0 \quad \text{Eq. (20)}$$

Eq. (20) assumes a constant flow rate throughout the column which would be strictly true only for the case of an infinitely dilute solute. Since the system of interest was extremely dilute and incompressible, the equation given above does apply. The above equation can be further reduced if the following transformations are used

$$\theta = t - Z/\sqrt{u} \quad \text{Eq. (21)}$$

$$X = Z/mV \quad \text{Eq. (22)}$$

Eq. (20) then becomes

$$\frac{\partial C}{\partial X} = - \frac{\partial q}{\partial \theta} \quad \text{Eq. (23)}$$

The above equation shows the rate of adsorption as a function of the concentration changes along the bed length.

External mass transfer through the stagnant film surrounding the adsorbent particle may be represented by

$$\frac{\partial q}{\partial \theta} = K_L a (C^* - C_s) \quad \text{Eq. (24)}$$

where a = mass transfer area

C^* = bulk adsorbate concentration

C_s = equilibrium concentration at solid surface.

Intraparticle diffusion for a homogeneous particle is given by

$$\frac{\partial q_i}{\partial \theta} = DV^2 q_i = D \frac{\partial}{\partial r} \left(r^2 \frac{\partial q_i}{\partial r} \right) \quad \text{Eq. (25)}$$

with initial and boundary conditions

$$\text{IC I} \quad q_i(r, X, \theta) = 0 \quad \text{at } \theta = 0 \quad 0 \leq r \leq R_0 \quad \text{Eq. (25-a)}$$

$$\text{BC I} \quad \phi = C/C_0 = 0 \quad \text{at } X = 0 \quad t \leq 0 \quad \text{Eq. (25-b)}$$

$$\text{BC II} \quad \phi = C/C_0 = 1 \quad \text{at } X = 0 \quad t \geq 0 \quad \text{Eq. (25-c)}$$

Assuming the diffusion rate is radially dependent only, the overall average diffusion throughout the particle may be found by integrating over the particle volume

$$q(X, \theta) = \frac{\int_0^R q_i(r, X, \theta) r^2 dr}{\int_0^R r^2 dr} = \frac{3}{R^3} \int_0^R q_i(r, X, \theta) r^2 dr \quad \text{Eq. (26)}$$

Eq. (23) was used as the starting point for the generation of diffusion controlled breakthrough curves for systems exhibiting Langmuir type isotherms.

Eq. (25) may be solved for constant surface concentrations to give the series solution

$$H(r, \theta) = \frac{C - C_1}{C_0 - C_1} = 1 + \frac{2R}{\pi r} \sum_{n=1}^{\infty} \frac{(-1)^n}{n} \sin(\sigma_n r) e^{-D\sigma_n^2 \theta} \quad \text{Eq. (27)}$$

where $\sigma_n = \frac{n\pi}{R}$

$H(r, \theta)$ is the solution of the problem of solid diffusion into an initially empty spherical particle.

After applying Duhamel's theorem to transform Eq. (27) to the case of varying surface concentrations, the result is substituted into Eq. (26). After interchanging the integration and summation so that the integration with respect to r may be carried out,

$$q = \frac{6D}{R^2} \sum_{n=1}^{\infty} \int_0^{\theta} q_s e^{-D\sigma_n^2(\theta-\lambda)} d\lambda \quad \text{Eq. (28)}$$

where λ is a dummy variable of integration. Leibnitz's rule for differentiating an integral may be employed to yield

$$\frac{\partial C}{\partial X} = - \frac{\partial q}{\partial \theta} = - \frac{6D}{R^2} \sum_{n=1}^{\infty} \int_0^{\theta} \frac{\partial q_s(X, \lambda)}{\partial \lambda} e^{-D\sigma_n^2(\theta-\lambda)} d\lambda \quad \text{Eq. (29)}$$

Eq. (29) has only two unknowns, and to get the concentration profile, one should obtain an expression for q_s in terms of C .

Rosen (27) evaluated q_s from Eq. (24) and (25) to obtain

$$\frac{\partial q_s}{\partial \lambda} = K_D \left[\frac{\partial C}{\partial \lambda} + R_f \frac{\partial C}{\partial X} \right] \quad \text{Eq. (30)}$$

In 1952 Rosen published an analytical solution to Eq. (29) assuming a linear isotherm. The generated breakthrough curves were used to calculate diffusion coefficients and external mass transfer coefficients.

Rosen's basic approach was followed by Antonson (4) in obtaining theoretical curves valid for systems that could be represented by a Langmuir type of equilibrium isotherm. When q_s is eliminated from Eq. (29) by use of the Langmuir isotherm,

$$q^* = \frac{a_1 C^*}{1 + a_2 C^*} \quad \text{Eq. (4)}$$

and the resulting expression substituted into the fluid phase mass balance, expressed as Eq. (23), the result is Eq. (31).

$$\frac{\partial C}{\partial X} = -\frac{6}{R^2} \sum_{n=1}^{\infty} \int_0^{\theta} \frac{\partial}{\partial X} \left(\frac{a_1 C^*}{1 + a_2 C^*} \right) \exp\left[-D \left(\frac{n\pi}{R}\right)^2 (\theta - \lambda)\right] d\lambda \quad \text{Eq. (31)}$$

Defining $\phi = C/C_0$, $\theta_T = \frac{2D}{R} \theta$, $\eta = \frac{3Da_1}{mVR^2}$, Eq. (31) becomes

$$\frac{\partial \phi}{\partial \eta} = -2 \sum_{n=1}^{\infty} \frac{\partial (\phi / (1 + a_2 C^*))}{\partial \lambda} e^{-1/2 n^2 \pi^2 (\theta_T - \lambda)} d\lambda \quad \text{Eq. (32)}$$

The above equation was used as the starting point for solution by numerical methods. A computer program which duplicates Antonson's numerical solution was used and values of C/C_0 were generated as a function of θ and η . The use of the generated breakthrough curves in fitting experimental data is described in the results section along with graphs of the computer printouts.

EQUIPMENT AND PROCEDURE

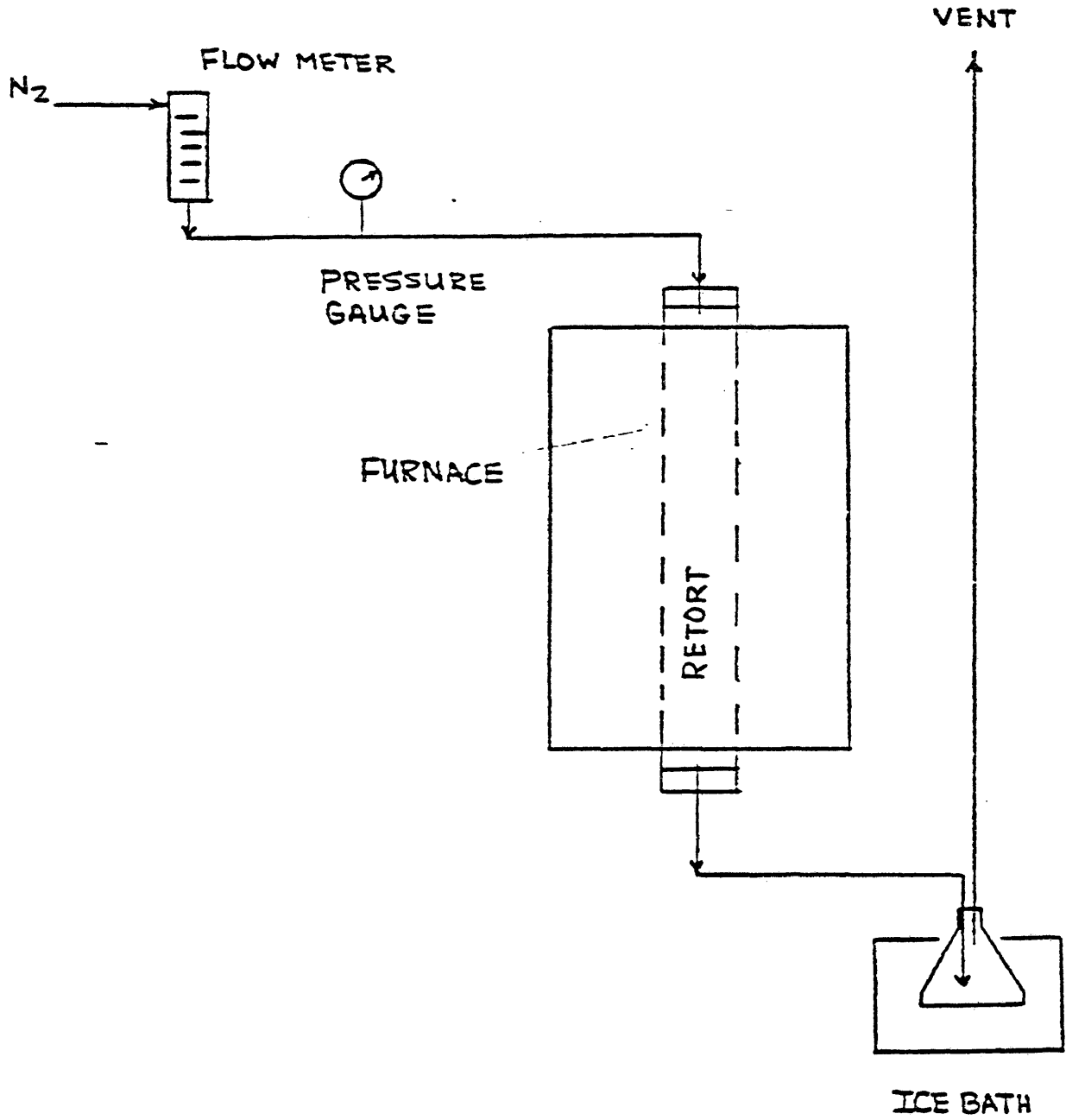
Adsorbent Preparation

Samples of raw shale were obtained from Laramie, Wyoming, and the material used contained 35 gallons of oil per ton of shale as found by Fischer Assay. A large quantity of raw shale was ground and mixed several times so that the effects of retorting temperature would not be masked by variations in properties of raw shale. The samples were sieved and the shale which passed a one-fourth inch screen but were collected on a one-eighth inch screen provided a homogeneous material for this study.

The retorting and production of spent shale was carried out in a 2 foot long stainless steel retort with an inside diameter of 2 inches. The retort as shown in figure 1, was sealed with threaded caps that had been tapped at each end to allow for the removal of oil and combustion gases and to provide a means of controlling the atmosphere inside the retort. Oil shale was packed into the retort which was then sealed and placed in a furnace. Nitrogen was passed through the retort at a rate of $15 \text{ cm}^3/\text{min}$ to provide an inert atmosphere while retorting. The retort was then heated to the desired retorting temperature and then the samples were re-torted for a fixed period of time. The retort was then cooled to ambient temperature while nitrogen continued to flow. As the processed samples were collected, they were crushed and

Schematic of Oil Shale Retort

Figure (1)



sieved to the desired size (20/40 US mesh). The samples then were analyzed for residual carbon, hydrogen, nitrogen, sulfur, and heat content. In addition, an X-ray diffraction analysis of each sample was conducted to determine the effects of re-torting temperature on the mineral contents of the processed shale.

Adsorption Equipment

The experimental apparatus was designed and constructed to utilize an ultraviolet detector to measure and record gas concentrations. The apparatus, shown in figure 2, consisted of the following.

Constant temperature bath

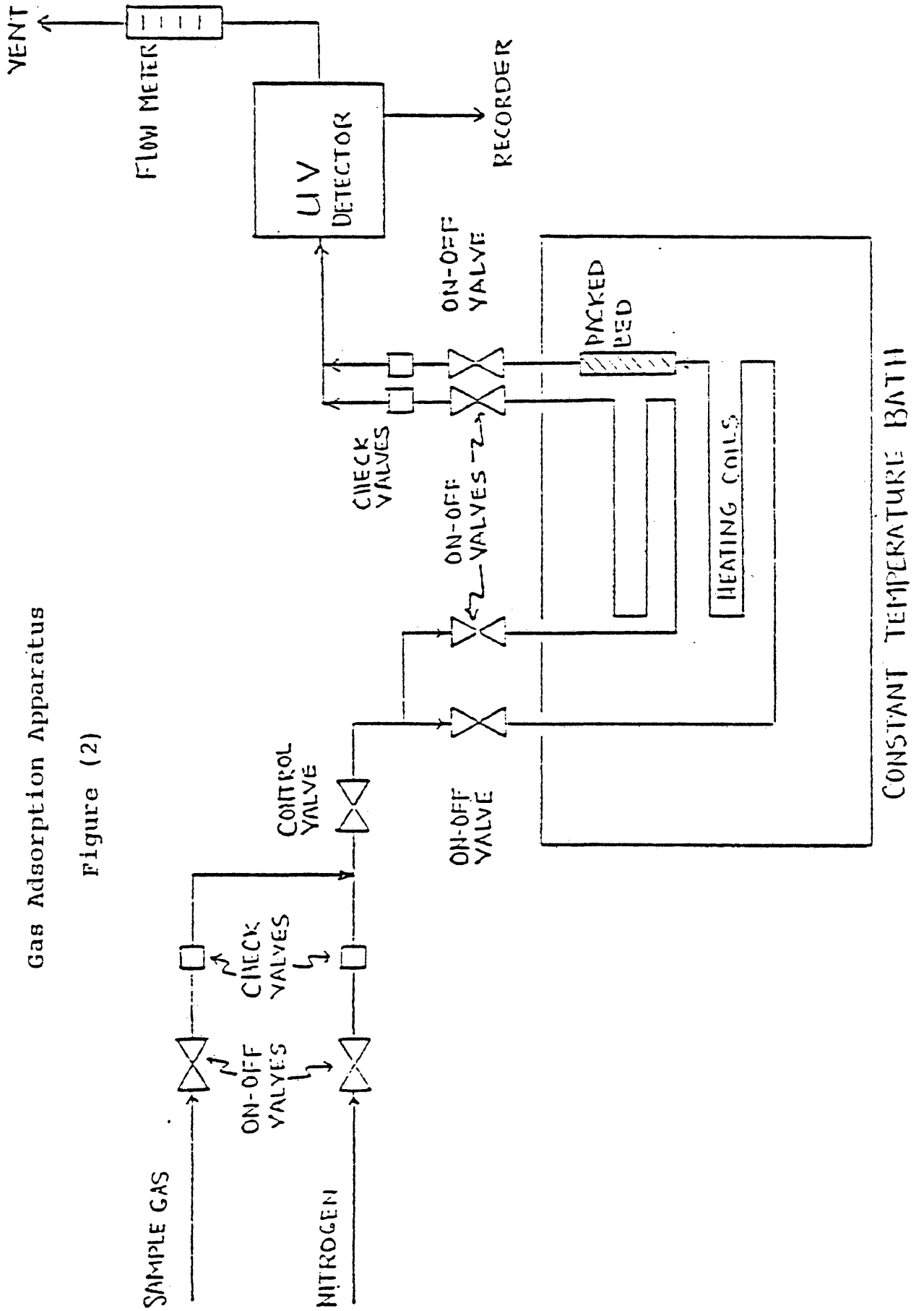
A refrigeration-heating cycle water bath was used. The water temperature in the bath was automatically controlled to desired temperature, and also it was checked from time to time by a regular thermometer to assure a constant temperature during the experimental run.

Heating coils

Heating coils were used to allow for the adsorbate to reach the desired temperature. Since the gas heat transfer coefficient is relatively low (in order of $50 \frac{\text{BTU}}{\text{FT}^2 \cdot \text{F}}$), a 60 ft long heating coil was used. The coil was made from a 1/8 in. OD stainless steel tube.

Gas Adsorption Apparatus

Figure (2)



Flow Meter

The gas flow rate was continuously monitored with a rotameter type of flow measuring device which had been calibrated to experimental conditions. The calibration curve was obtained using a soap bubble flow meter and is given in Appendix C. Because of the sensitivity of flow rates to adsorption data, flow rates were checked periodically with a soap bubble meter to insure steady flow conditions.

Ultraviolet detector

The effluent gas concentration was continuously monitored with a Beckman model 25 ultraviolet detector. A scan of the wavelength was performed from the visible to the ultraviolet region in order to obtain the highest wavelength peak. This was 198Å which is in the ultraviolet region. The detector was hooked to a chart recorder which gave a constant chart speed that ranged from 0.1 in/min-10 in/min.

Packed column

The column used in this study was prepared from a 1/2 in OD stainless steel tube 7.5 inches in length. It was furnished with union reducers at both ends to make it easy to be hooked to one end of the heating coil and the other end to the UV detector. Packing the column to insure a constant amount of material for each run was considered to be an important part of the procedure. Each end of the column section contained a 1/4 in section of pyrex glass wool to prevent small particles of spent shale from being carried away by the gas flow.

Experimental procedure

After the column was packed and placed in the constant temperature bath, pure nitrogen gas was passed through the packed bed to flush out any impurities and to establish a base line. The pure nitrogen gas was passed through the column until the bed and the gas reached thermal equilibrium. The gas flow rate of the SO₂-nitrogen mixture was then started and the effluent gas concentration was continuously monitored and recorded. The sample gas was continued until the effluent and inlet concentrations were equal. At the end of each run, the column was disassembled and a fresh sample was packed in the column for the next run.

RESULTS AND DISCUSSION

The results of the spent shale sample selection, effect of concentration and temperatures on the experimentally derived breakthrough curves and isotherms, and the heat of adsorption calculated from equilibrium isotherms are presented in this section along with the computer generated breakthrough curves as fitted to the experimental ones. Analysis of the experimental data yielded approximate values for the overall intraparticle diffusion coefficients.

Sample selection

Selection of spent shale on which to adsorb the gas was an important consideration because of the variation in shale properties found at different retorting temperatures and retorting times.

The chemical and X-ray diffraction analyses for all retorting times and temperatures are given in Tables I, II, III, IV, V, and VI. Also a BET surface area analysis was performed on samples which were retorted at temperatures ranging from 300°C to 1000°C for 2 hours. The results are given as a function of retorting temperature in table VII and are shown graphically in figure 3.

Since it was noted that retorting temperature appears to more strongly influence the properties of the spent shale than does retorting time, material that had been retorted for two hours was used. The selection of the retorting temperature

Table I
 Chemical Analyses of Oil Shale Retorted for Two Hours

Retorting Temperature, °C	Weight Percent							Heat Content, Btu
	<u>Carbon</u>	<u>Hydrogen</u>	<u>Nitrogen</u>	<u>Sulfur</u>	<u>Carbon Dioxide</u>	<u>Mineral Carbon</u>	<u>Organic Carbon</u>	
300	14.15	1.32	0.58	0.62	17.75	4.84	9.31	2015.5
400	9.61	0.54	0.56	0.56	18.59	5.07	4.54	900.7
500	7.55	0.16	0.46	0.48	18.70	5.10	2.45	254.1
600	7.24	0.15	0.45	0.50	18.24	4.98	2.26	355.9
700	5.94	0.09	0.42	0.51	14.38	3.98	2.02	289.3
800	4.94	0.12	0.33	0.57	9.57	2.61	2.33	351.4
900	1.02	0.08	0.23	0.64	1.45	0.40	0.62	133.8
1000	0.40	0.01	0.14	0.65	0.66	0.18	0.22	--

Table II
 Chemical Analyses of Oil Shale Retorted for Five Hours

Retorting Temperature, °C	Weight Percent							Heat Content, Btu
	Carbon	Hydrogen	Nitrogen	Sulfur	Carbon Dioxide	Mineral Carbon	Organic Carbon	
300	13.62	1.22	0.60	0.51	18.11	4.94	8.68	2064
400	10.99	0.83	0.55	0.47	19.28	5.26	5.73	2017
500	7.41	0.08	0.48	0.46	19.86	5.42	1.99	1099
600	6.62	0.24	0.46	0.46	17.99	4.91	1.71	1059
700	4.06	0.22	0.36	0.59	9.01	2.46	1.60	665
800	3.19	0.07	0.23	0.59	6.34	1.73	1.46	455
900	1.19	0.07	0.14	0.54	1.71	0.47	0.72	148
1000	1.01	0.04	0.15	0.56	0.81	0.22	0.79	107

Table III
 Chemical Analysis of Oil Shale Retorted for Fifteen Hours

Retorting Temperature, °C	Weight Percent							Heat Content, Btu
	<u>Carbon</u>	<u>Hydrogen</u>	<u>Nitrogen</u>	<u>Sulfur</u>	<u>Carbon Dioxide</u>	<u>Mineral Carbon</u>	<u>Organic Carbon</u>	
300	4.65	1.43	0.66	0.58	17.65	4.82	nil	1366
400	11.72	0.84	0.60	0.51	18.98	5.18	6.54	2136
500	7.86	0.28	0.50	0.45	19.60	5.35	2.31	1267
600	6.73	0.08	0.43	0.44	18.05	4.93	1.80	994
700	4.68	0.08	0.32	0.51	11.45	3.12	1.56	684
800	1.86	0.15	0.24	0.52	3.45	0.94	0.92	291
900	1.05	0.09	0.21	0.57	0.96	0.26	0.79	140
1000	0.65	0.03	0.20	0.49	0.29	0.08	0.57	45

Table IV
 X-Ray Diffraction Analysis of Shale Samples
 Retorted for Two Hours

Retorting Temperature, °C	Weight Percent		Sodium Potassium		Melillite Diopside Periclase				
	Quartz	Calcite	Dolomite	Analcite	Feldspar	Feldspar	Melillite	Diopside	Periclase
300	10	3	31	*	*	*	-	-	-
400	11	3	34	*	*	*	-	-	-
500	11	4	31	*	*	*	-	-	-
600	11	5	27	*	*	*	-	-	-
700	11	7	11	*	*	*	-	-	*
800	10	7	9	*	*	*	-	-	*
900	7	-	-	-	*	*	*	*	*
1000	5	-	-	-	*	*	*	*	*

*mineral present

Table V

X-Ray Diffraction Analysis of Shale Samples
Retorted for Five Hours

Retorting Temperature, °C	Weight Percent			Sodium		Potassium	
	Quartz	Calcite	Dolomite	Analcite	Feldspar	Feldspar	Mellitite Diopside Periclase
300	12	3	32	*	*	*	-
400	11	3	37	*	*	*	-
500	11	3	33	*	*	*	-
600	10	5	27	*	*	*	-
700	10	6	4	*	*	*	*
800	9	4	6	-	*	*	*
900	9	-	-	-	*	*	*
1000	6	-	-	-	*	*	*

*mineral present

Table VI
 X-Ray Diffraction Analysis of Shale Samples
 Retorted for Fifteen Hours

Retorting Temperature, °C	Weight Percent			Sodium Potassium			Melillite Diopside Periclase		
	Quartz	Calcite	Dolomite	Analcite	Feldspar	Feldspar	Melillite	Diopside	Periclase
300	11	3	33	21	*	*	-	-	-
400	11	4	34	19	*	*	-	-	-
500	11	4	35	18	*	*	-	-	-
600	11	5	26	9	*	*	-	-	-
700	11	6	10	8	*	*	*	*	*
800	9	2	4	5	*	*	*	*	*
900	7	-	-	-	*	*	*	*	*
1000	5	-	-	-	*	*	*	*	*

*mineral present

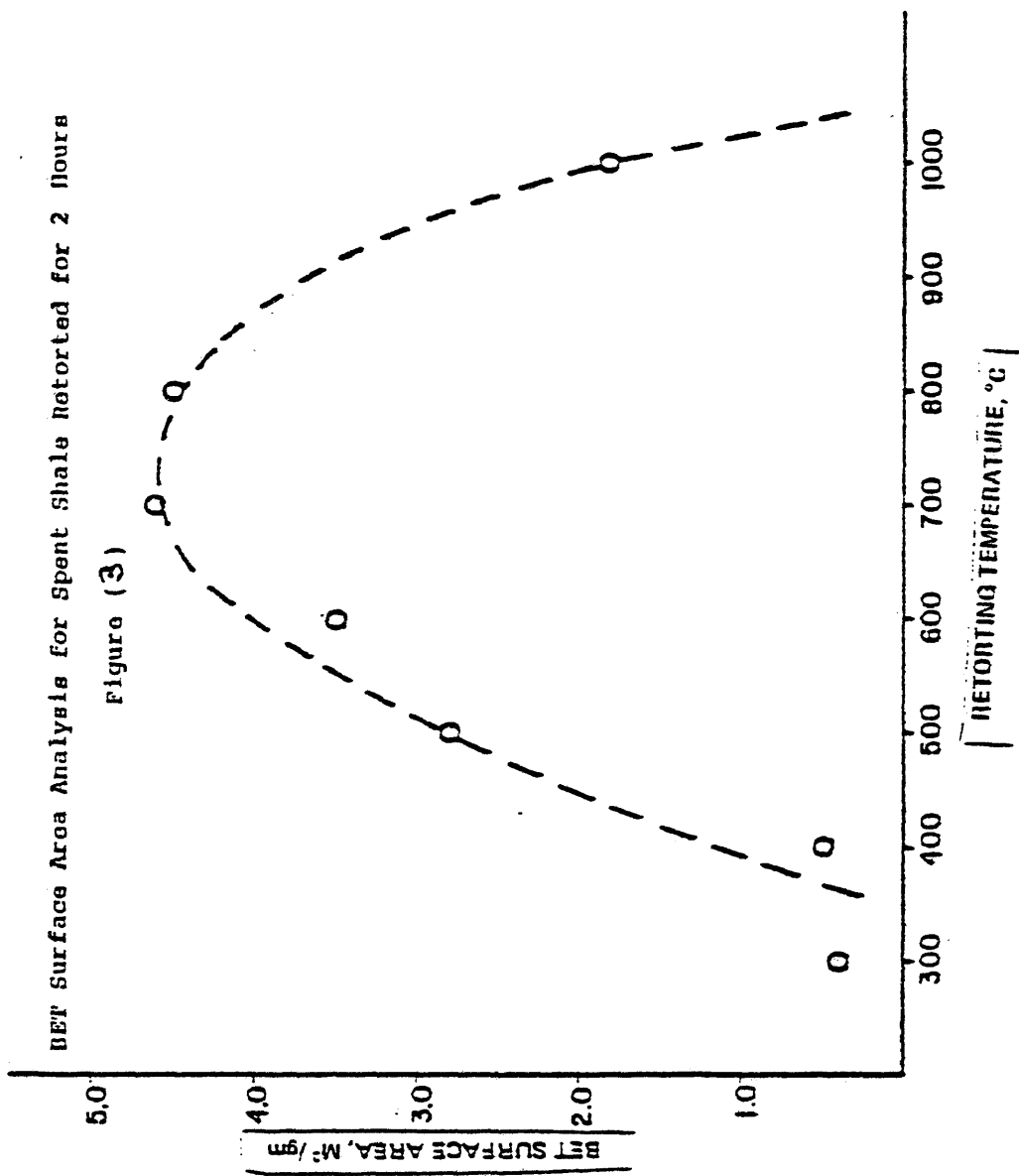
TABLE VII

BET Surface Area of Spent Shale
Which Was Retorted at Different Temperature

Retorting Temperature, °C	BET Surface Area m ² /gm
300°C	0.4
400°C	0.5
500°C	2.8
600°C	3.5
700°C	4.6
800°C	4.5
900°C	3.0
1000°C	1.8

BET Surface Area Analysis for Spent Shale Retorted for 2 Hours

Figure (3)



involved carrying out adsorption studies on shale that had been retorted at temperatures ranging from 300 to 1000°C. This was done by obtaining breakthrough curves with a sample gas containing 9704 PPM of SO₂ in nitrogen. The results are given in Table VIII on a per gram basis and are shown graphically in figure 4. As seen in the figure, the maximum SO₂ uptake occurs between 600 and 700°C. The chemical analysis in Table I shows that the spent shale contains only about 6% residual carbon at that temperature, but the percent of mineral carbon begins to decrease. Although the uptake of SO₂ was expected to decrease with decreasing residual carbon, this was not the case. The high uptake at 700°C can probably be attributed to the structural changes in the shale that results from the reaction of calcite and dolomite.

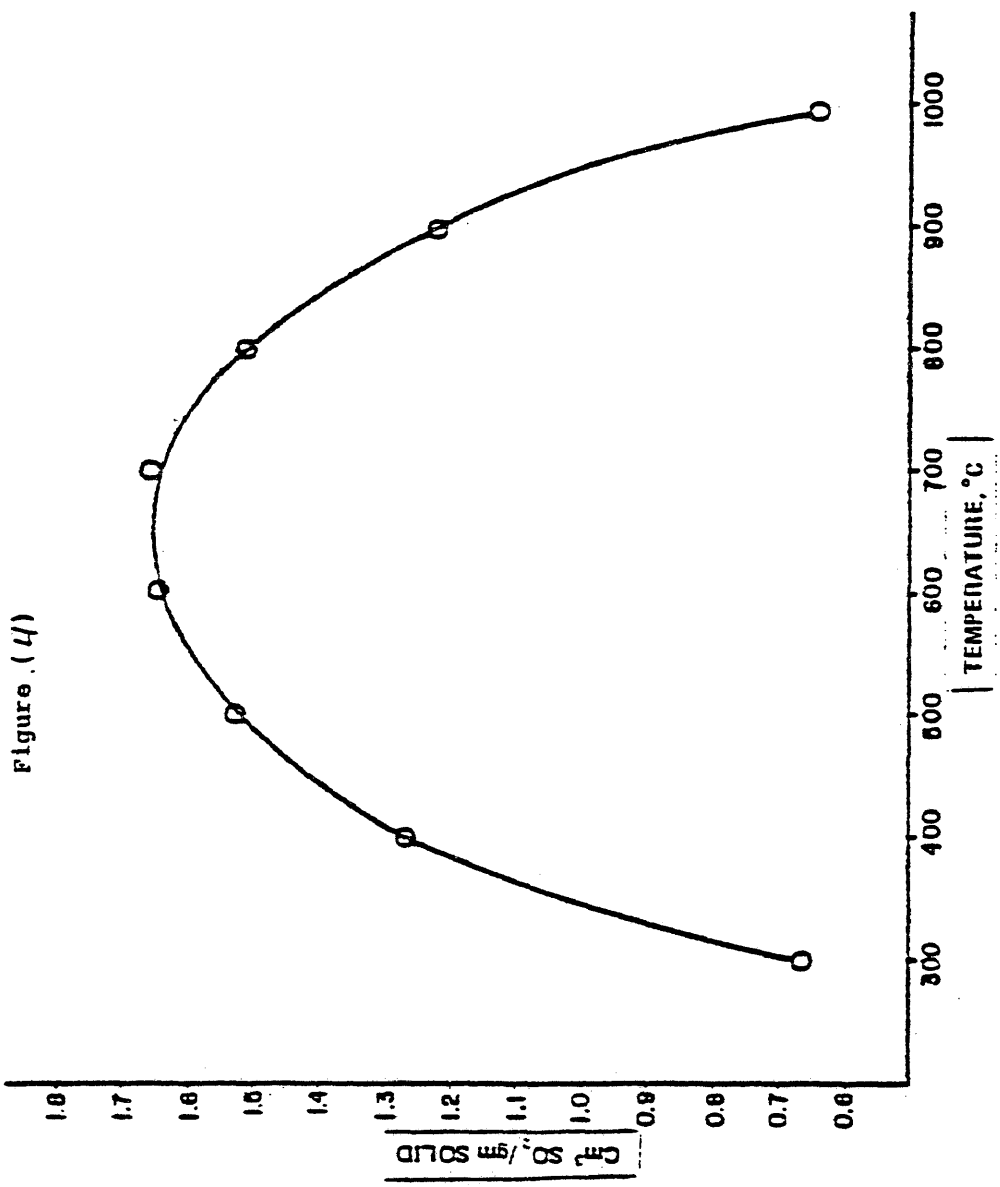
After selecting 700°C, experimental breakthrough curves were measured at 10°C, 27°C, and 40°C for concentrations of 993, 1999, 2999, 4998, 7226, and 9704 PPM of SO₂ in nitrogen. Replicate runs were necessary to calculate average breakthrough curves because of the nonhomogeneous nature of the spent shale.

Table VIII

Adsorption of SO₂ on Spent Shale at 27°C
Using a Concentration of 9706 PPM SO₂ in Nitrogen

<u>Retorting Temperature °C</u>	<u>cm³ SO₂/gm solid</u>
300	0.6658
400	1.2791
500	1.5431
600	1.6623
700	1.6732
800	1.5265
900	1.2340
1000	0.6424

Adsorption of SO₂ on Spent Shale Retorted at Temperatures Ranging from 300 to 1000°C



Effect of temperature and concentration on breakthrough curves

The effect of concentration on the experimentally obtained breakthrough curves are shown in figures 5, 6, 7, 8, 9, and 10. The effects of temperature are shown in figure 11. The higher the gas concentration used in this experiment the sooner the break point appears and vice versa; also as the temperature increases the break point occurs sooner.

Equilibrium isotherms

The equilibrium isotherms were calculated from the experimental breakthrough curves. The area above each breakthrough curve was measured using a planimeter. An average of three readings was considered. The amount of gas adsorbed in each run for a specific adsorbate concentration was then calculated. The relation between adsorbate concentration and amount of gas adsorbed on adsorbent was obtained by fitting the results to Langmuir, Freundlich, Polanyi and Dubinin types of relations. Making use of the fact that most of the mentioned relations can result in a straight line equation if a certain technique is used, the least square fit was then safely used to correlate the data with each relation.

Langmuir type of isotherm,

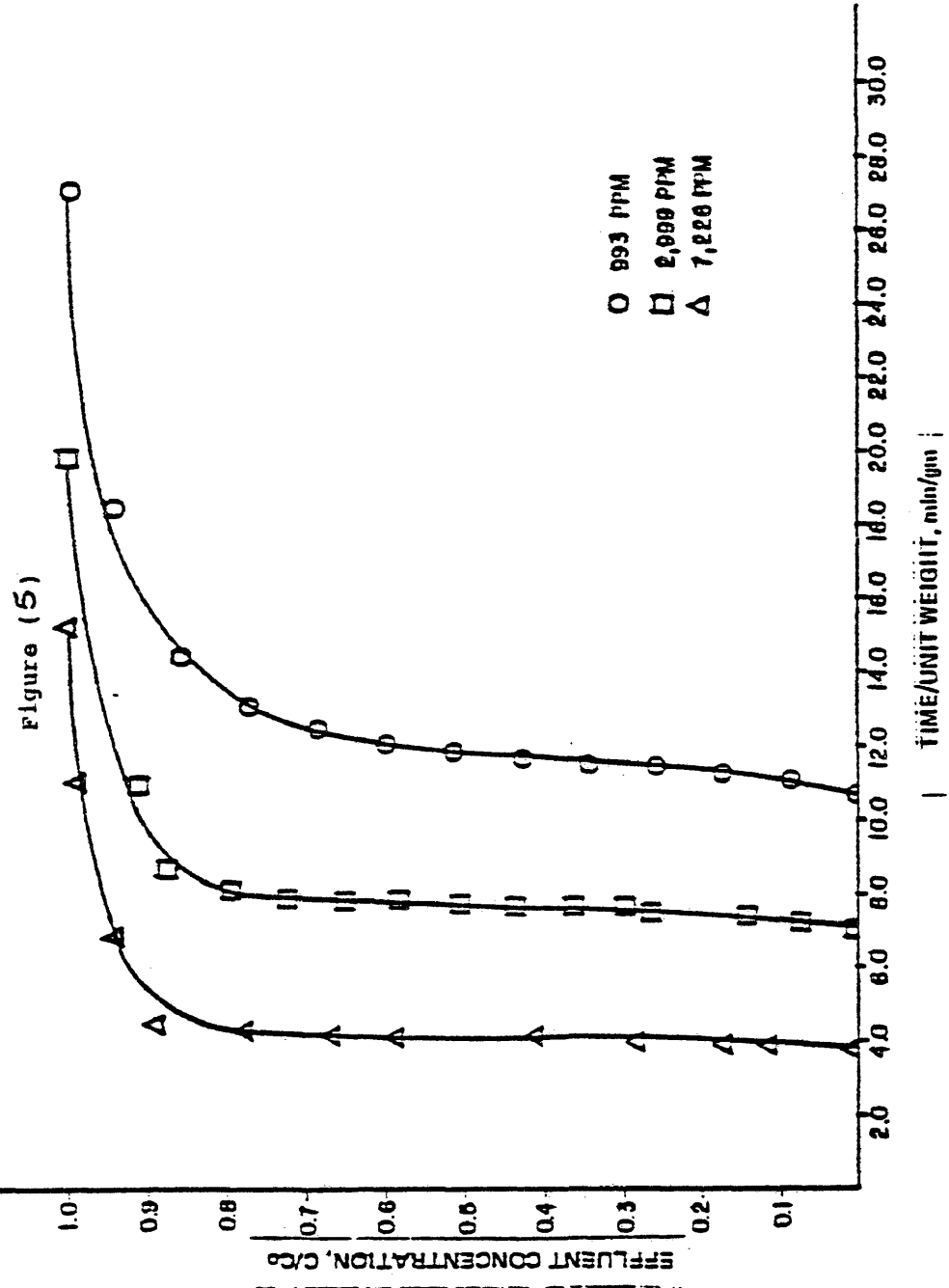
$$q^* = \frac{a_1 C^*}{1 + a_2 C^*} \quad \text{Eq. (4)}$$

can be rearranged to give

$$\frac{1}{q^*} = \frac{1}{a_1 C^*} + \frac{a_2}{a_1} \quad \text{Eq. (33)}$$

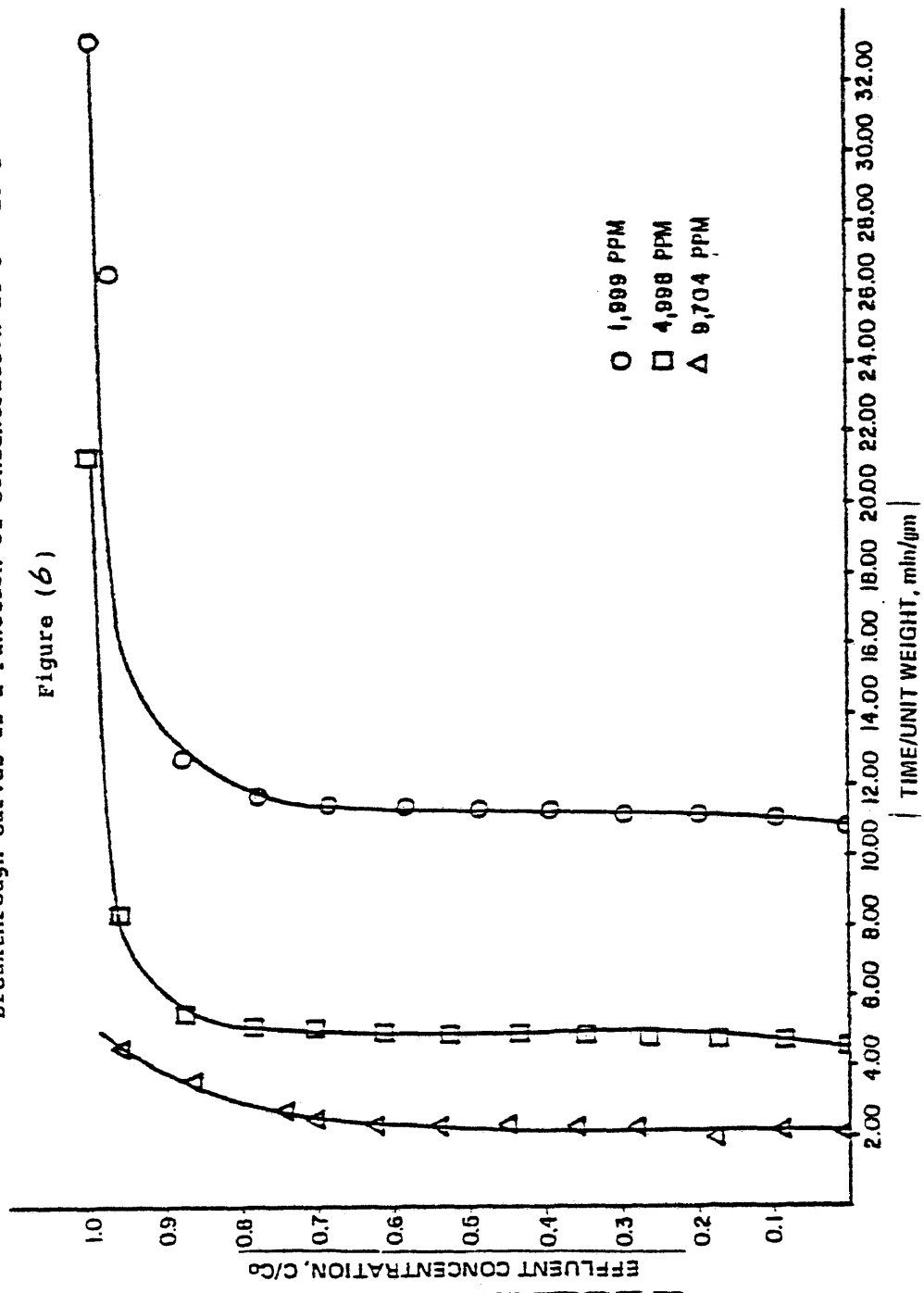
Equation (33) is in a suitable form for testing the experimental data. Plots of $\frac{1}{q^*}$ against $\frac{1}{C^*}$ would yield a straight line. It

Breakthrough Curves as a Function of Concentration at T = 10°C

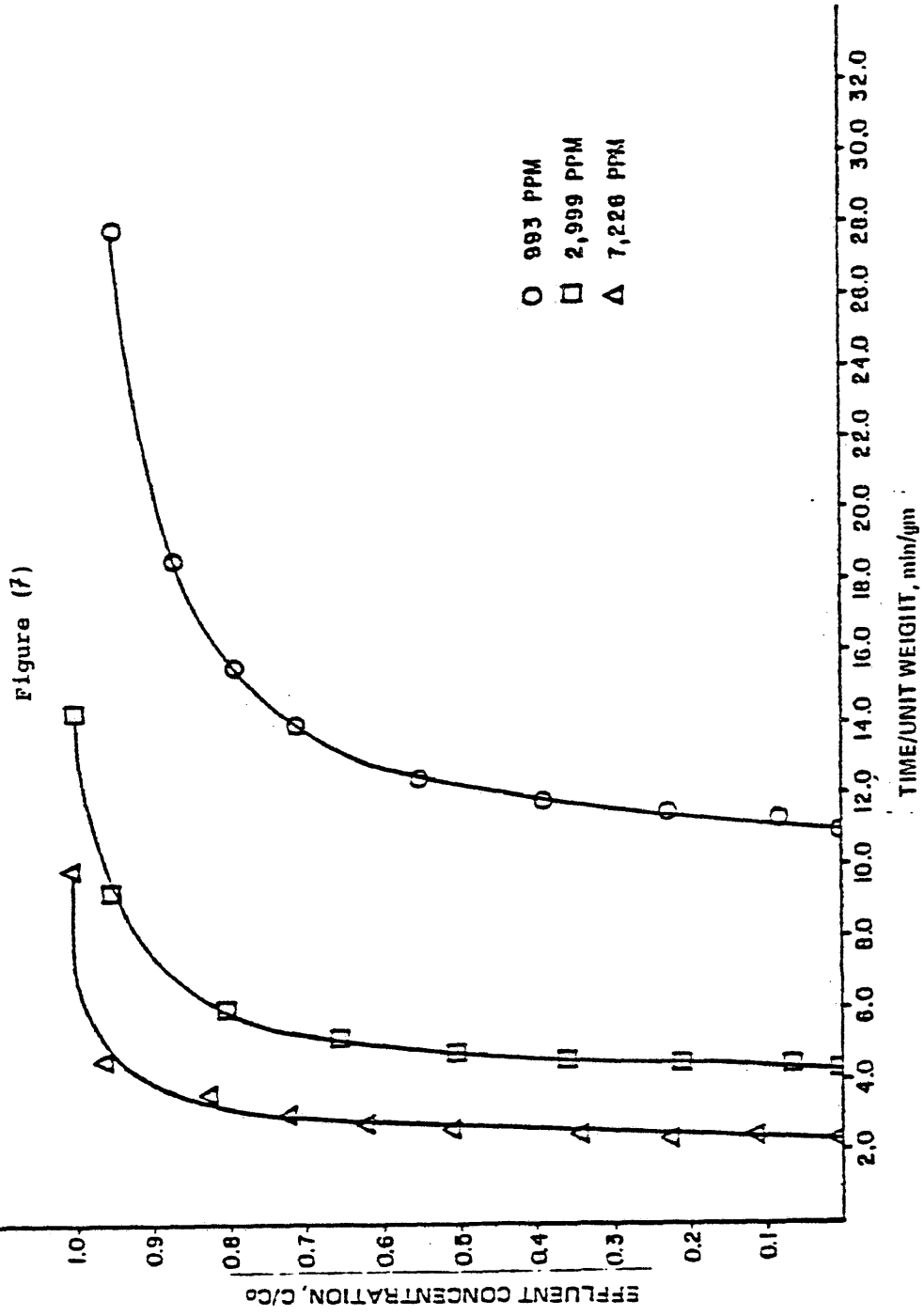


Breakthrough Curves as a Function of Concentration at T = 10°C

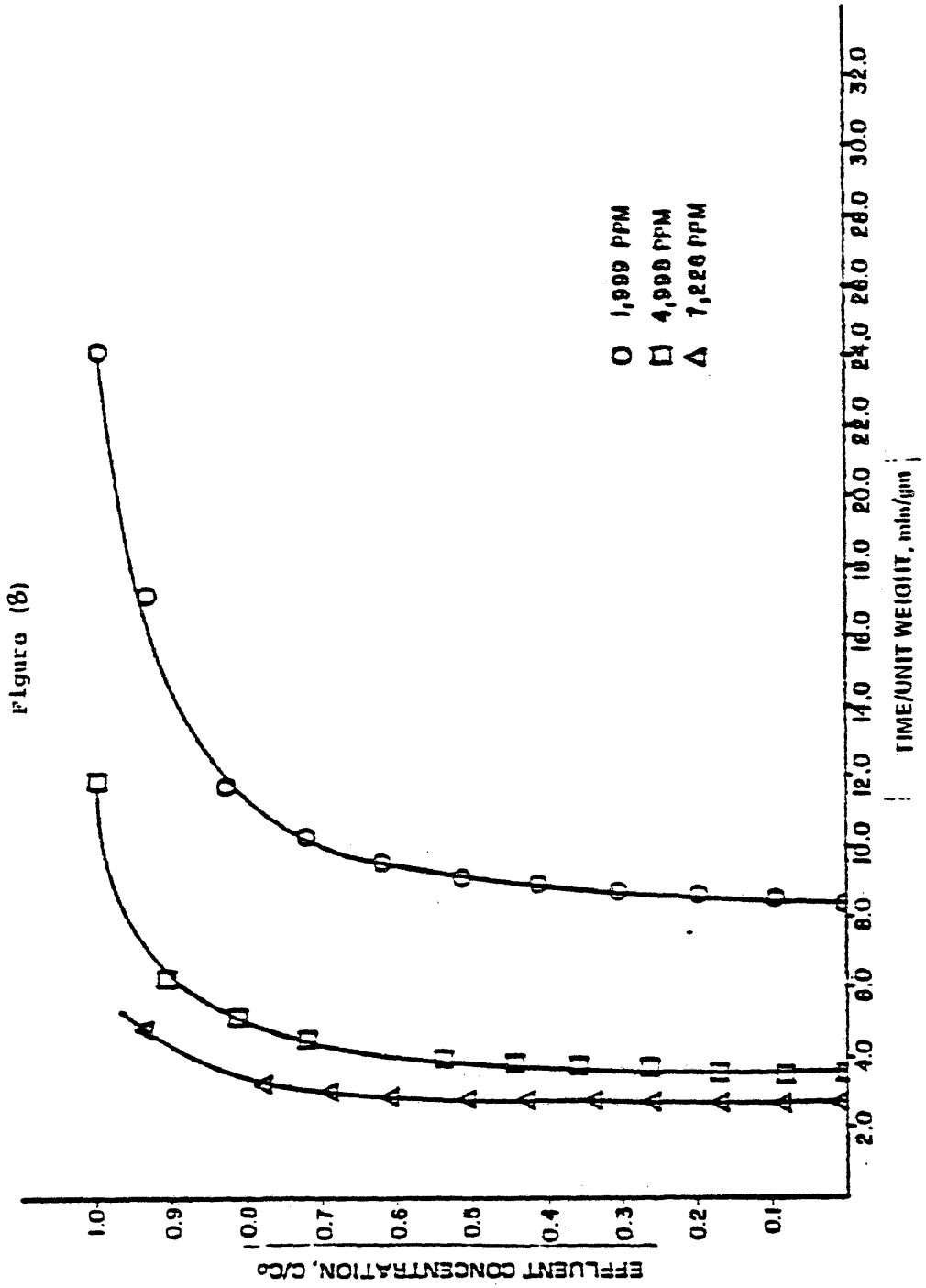
Figure (b)



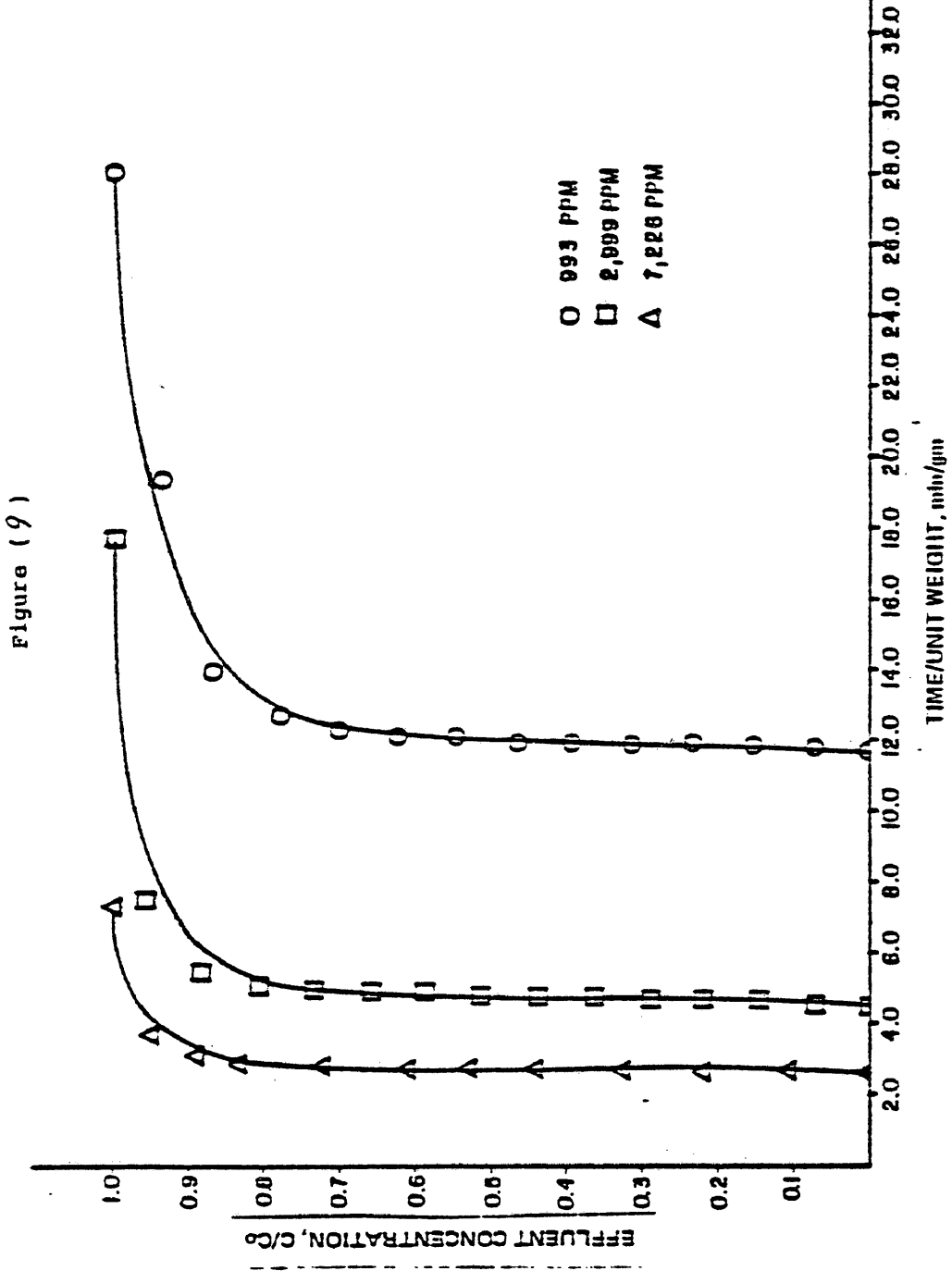
Breakthrough Curves as a Function of Concentration at T = 27°C



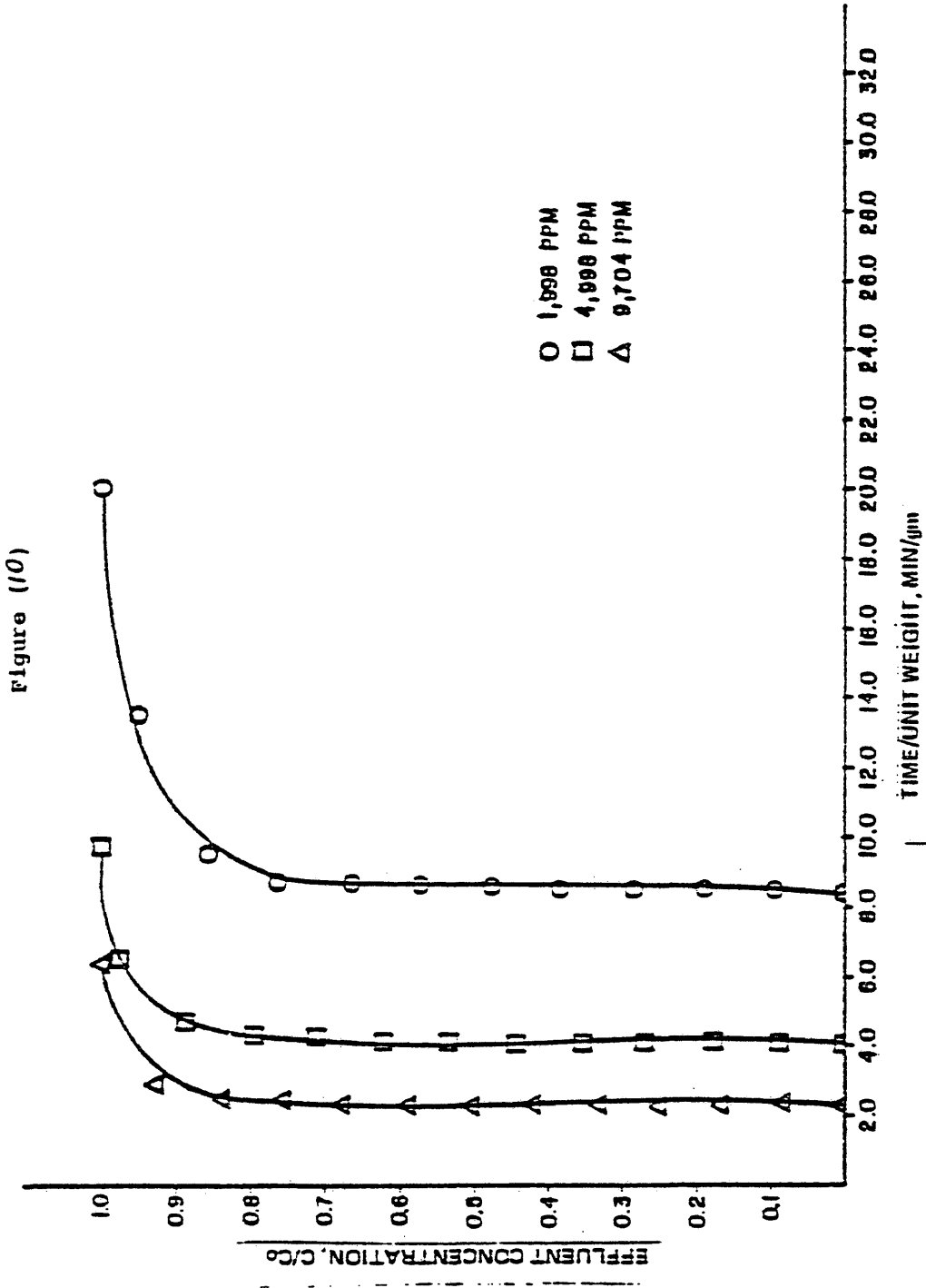
Breakthrough Curves as a Function of Concentrations at $T = 27^{\circ}\text{C}$



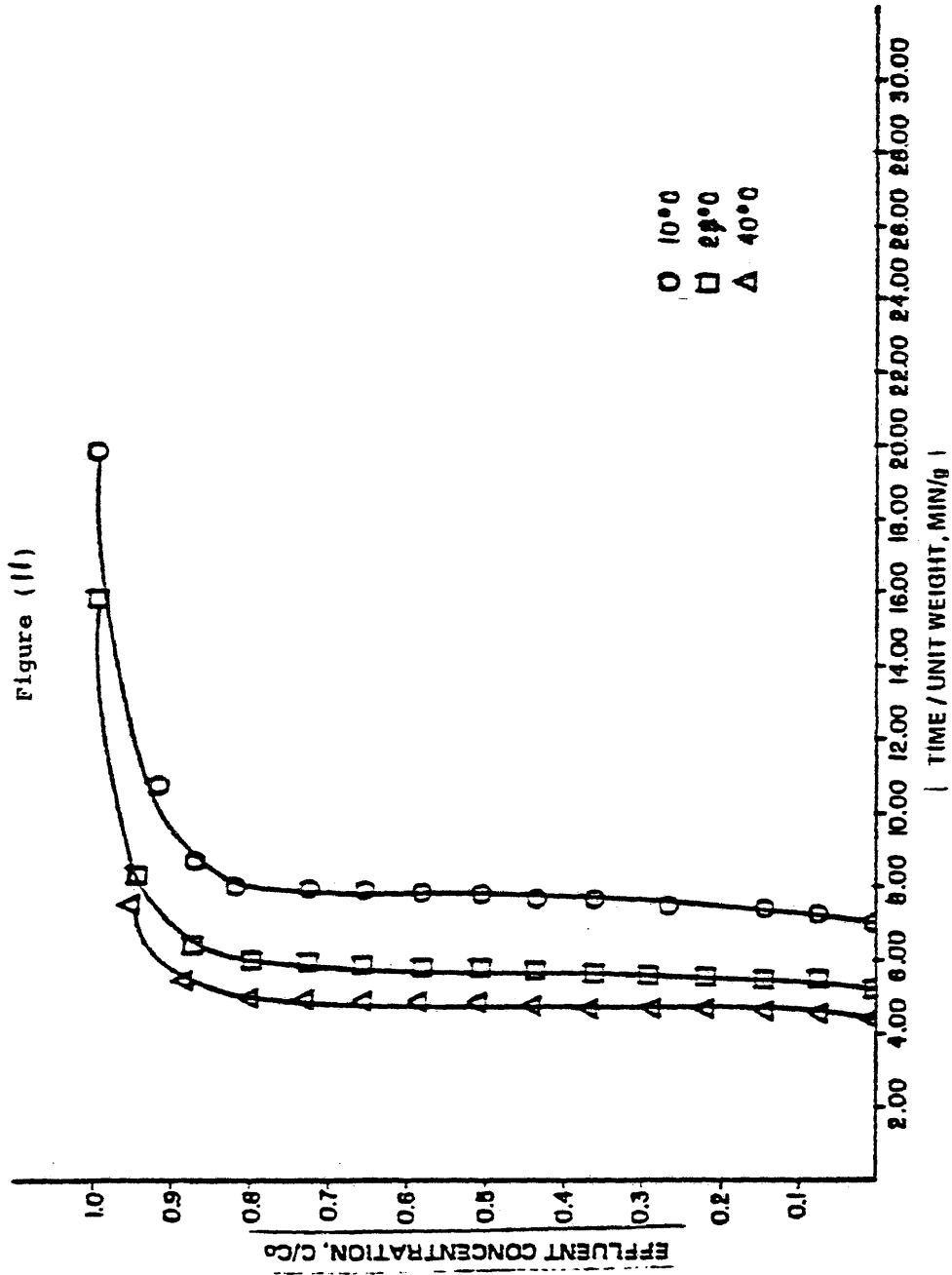
Breakthrough Curves as a Function of Concentration at T = 40°C



Breakthrough Curves as a Function of Concentration for T = 40°C



Breakthrough Curves as a Function of Temperature for $C_0 = 1999$ ppm SO_2 in N_2



must be emphasized, however, that obtaining a satisfactory straight line is a necessary but not a sufficient condition for the applicability of Langmuir's theory to the data in question. The least square curve fits for this equation are shown in figures 12, 13 and 14; the equilibrium isotherms data and Langmuir constants are given in table IX along with the calculated isotherms as shown in figure 15.

Freundlich type of isotherm,

$$q^* = K[C^*]^{1/n} \quad \text{Eq. (5)}$$

can be rearranged to give

$$\log q^* = 1/n \log C^* + \log K \quad \text{Eq. (34)}$$

The above equation can be plotted as $\log q^*$ vs $\log C^*$ to yield a straight line with slope of $1/n$ and intercept of $\log K$. The least square fits for this type of relation are shown in figure 16, 17 and 18. The equilibrium data and Freundlich constants are given in table X. The calculated equilibrium isotherm are compared in figure 19 to the equilibrium data.

The Dubinin equation, which is expressed as,

$$W = W_0 \exp \left[- \frac{a'}{\beta^2} \left(2.303RT \log_{10} \frac{P_0}{P} \right)^2 \right] \quad \text{Eq. (15)}$$

can be rearranged to give

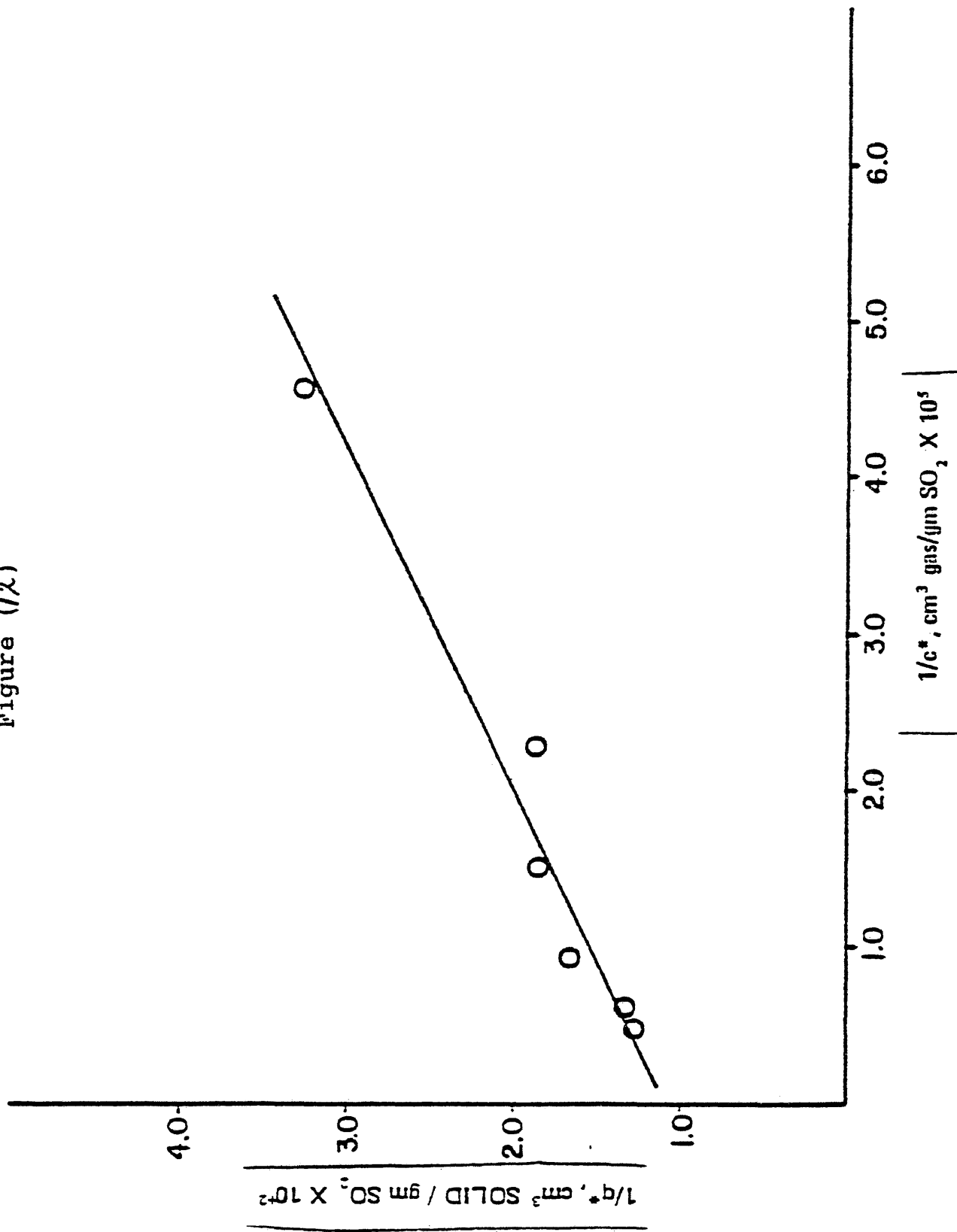
$$\log_{10} W = \log_{10} W_0 - B \left(\log_{10} \frac{P_0}{P} \right)^2 \quad \text{Eq. (16)}$$

where $B = 2.303 \frac{K}{\beta^2} (RT)^2$

This equation can be plotted as $\log_{10} W$ vs $\left(\log_{10} \frac{P_0}{P} \right)^2$ to yield a straight line with slope B and intercept of $\log W_0$. The least square fit for this isotherm is shown in figures 20, 21 and 22. The equilibrium data and the Dubinin constants are given in table XI.

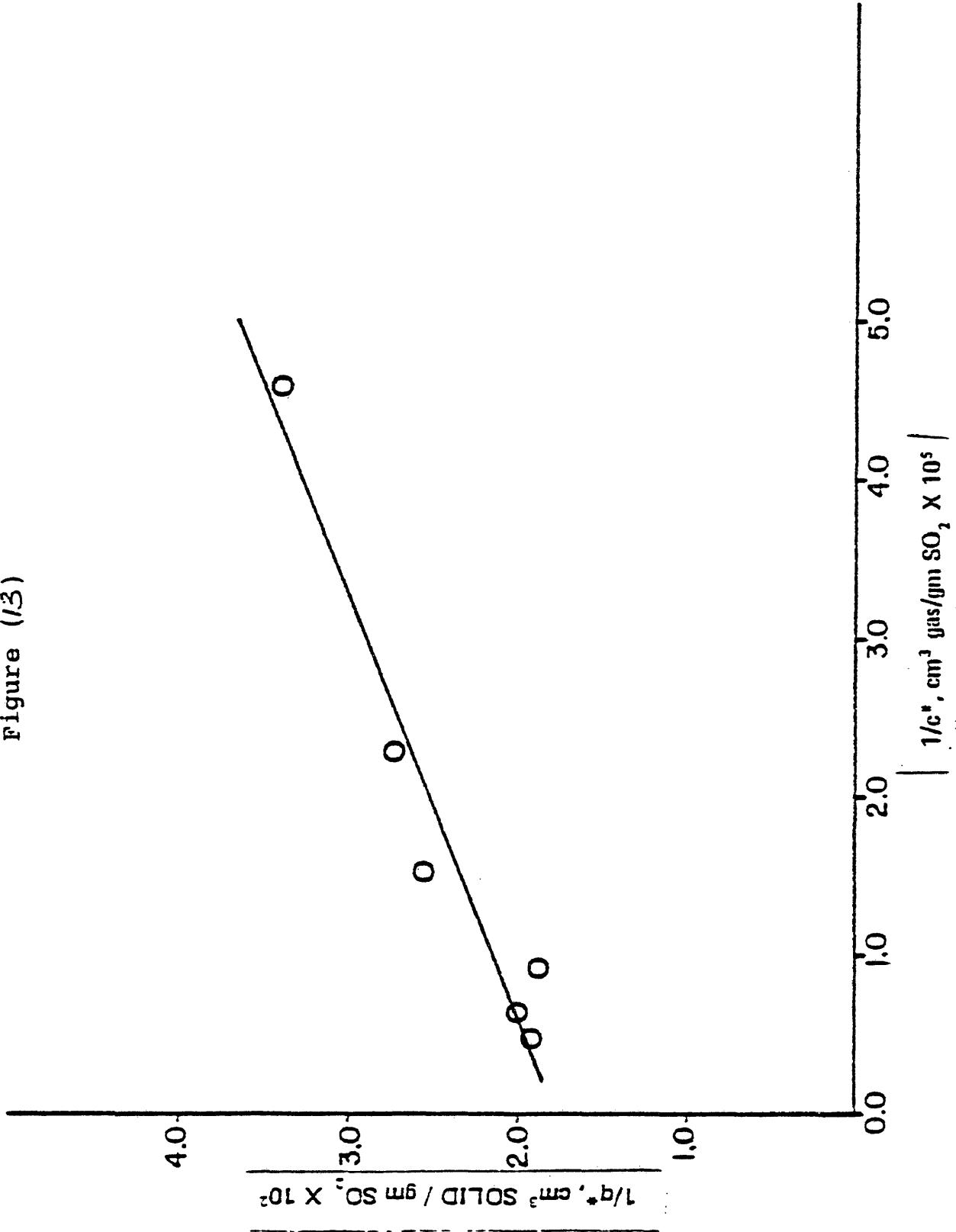
Least Square Fit to Langmuir Model at T = 10°C

Figure (12)



Least Square Fit for Langmuir Model at T = 27°C

Figure (13)



Least Square Fit for Langmuir Model at T = 40°C

Figure (14)

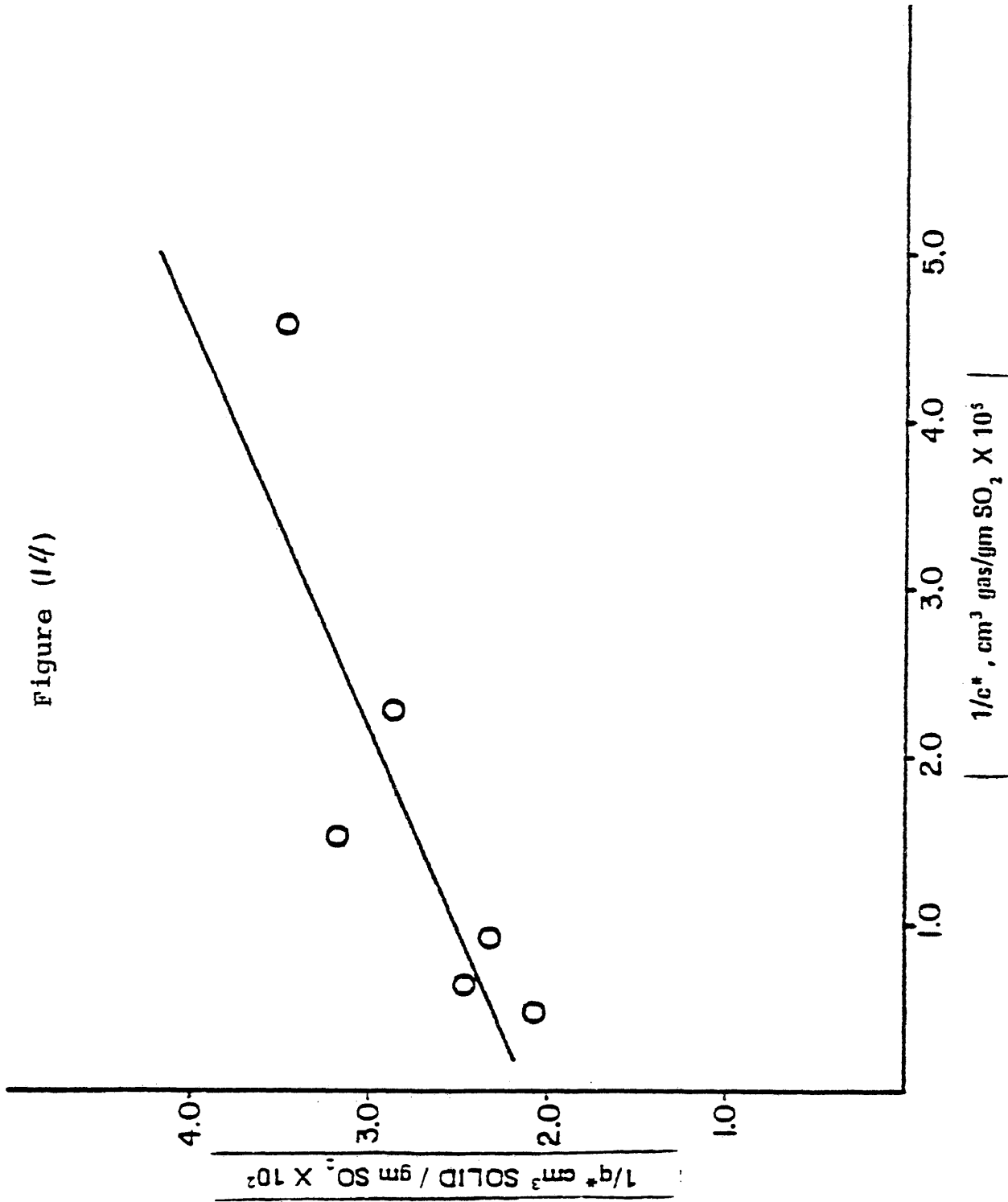


TABLE IX

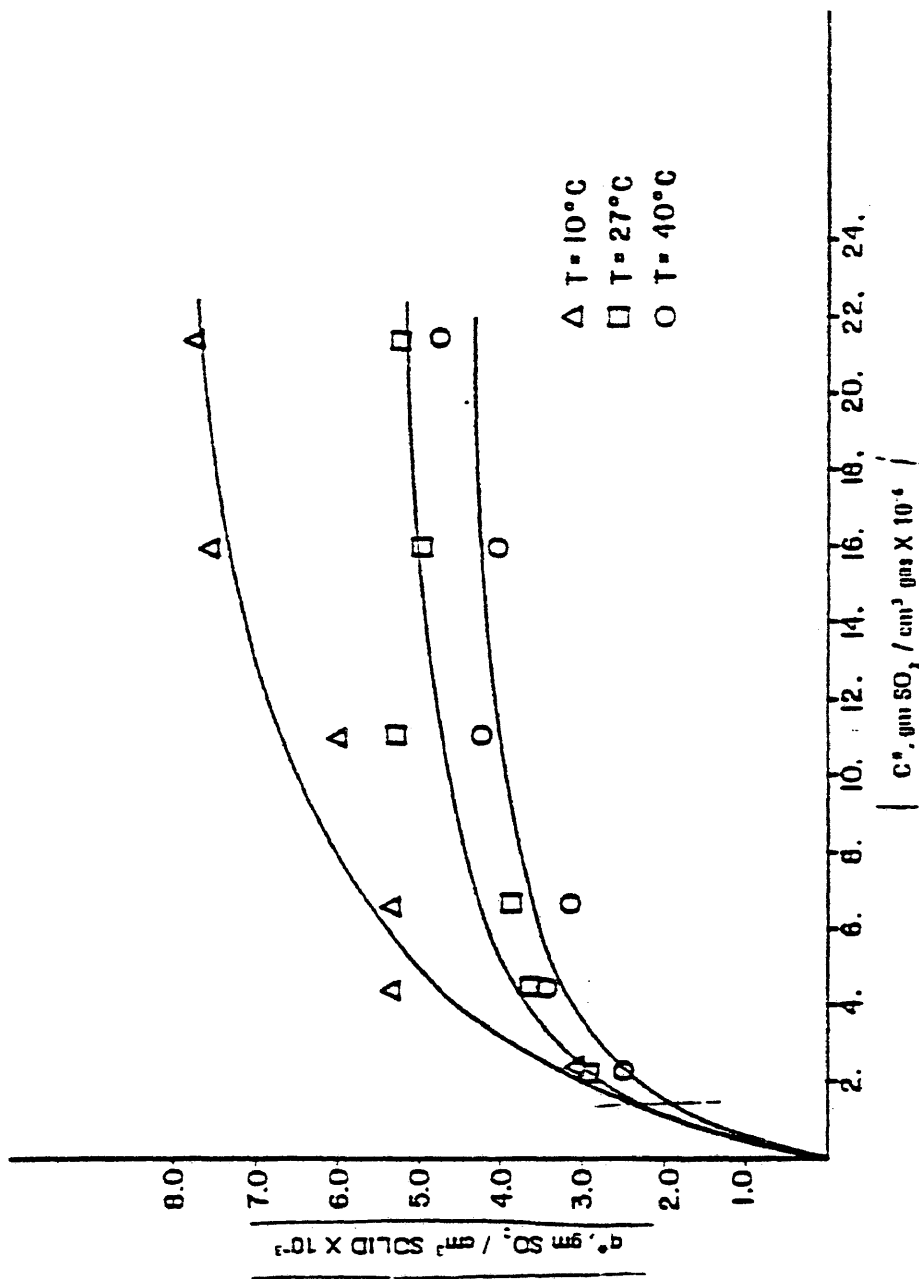
Equilibrium Isotherm Data and Langmuir Constants,
 a_1 and a_2 for SO_2 on Spent Shale

C^* , $\frac{\text{gm SO}_2}{\text{cm}^3 \text{ gas}} \times 10^{-6}$	q^* , $\text{mgm SO}_2/\text{cm}^3 \text{ solid}$		
	$T = 10^\circ\text{C}$	$T = 27^\circ\text{C}$	$T = 40^\circ\text{C}$
2.1866	3.0496	2.9350	2.5090
4.4018	5.3314	3.6609	3.4792
6.6038	5.3990	3.8920	3.1537
11.0056	6.0179	5,3093	4.2897
15.9117	7.5894	5.0032	4.0164
21.3682	7.7693	5.2481	4.7700

<u>Temperature, °C</u>	<u>a_2</u>	<u>a_1</u>
10	2.3184×10^5	2153.27
27	4.66802×10^5	2647.18
40	5.07126×10^5	2406.87

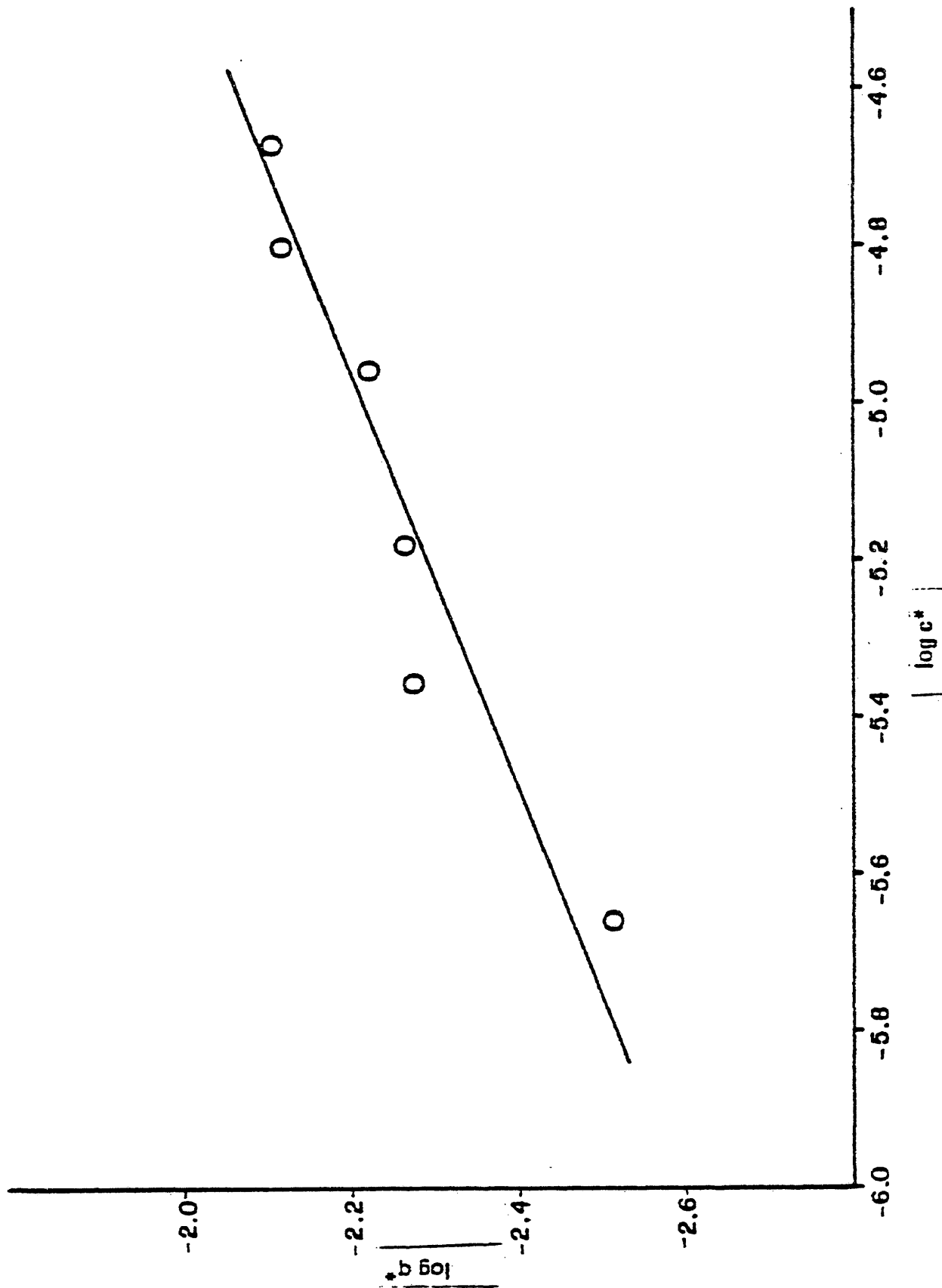
Equilibrium Data Fit to Langmuir Model

Figure (15)



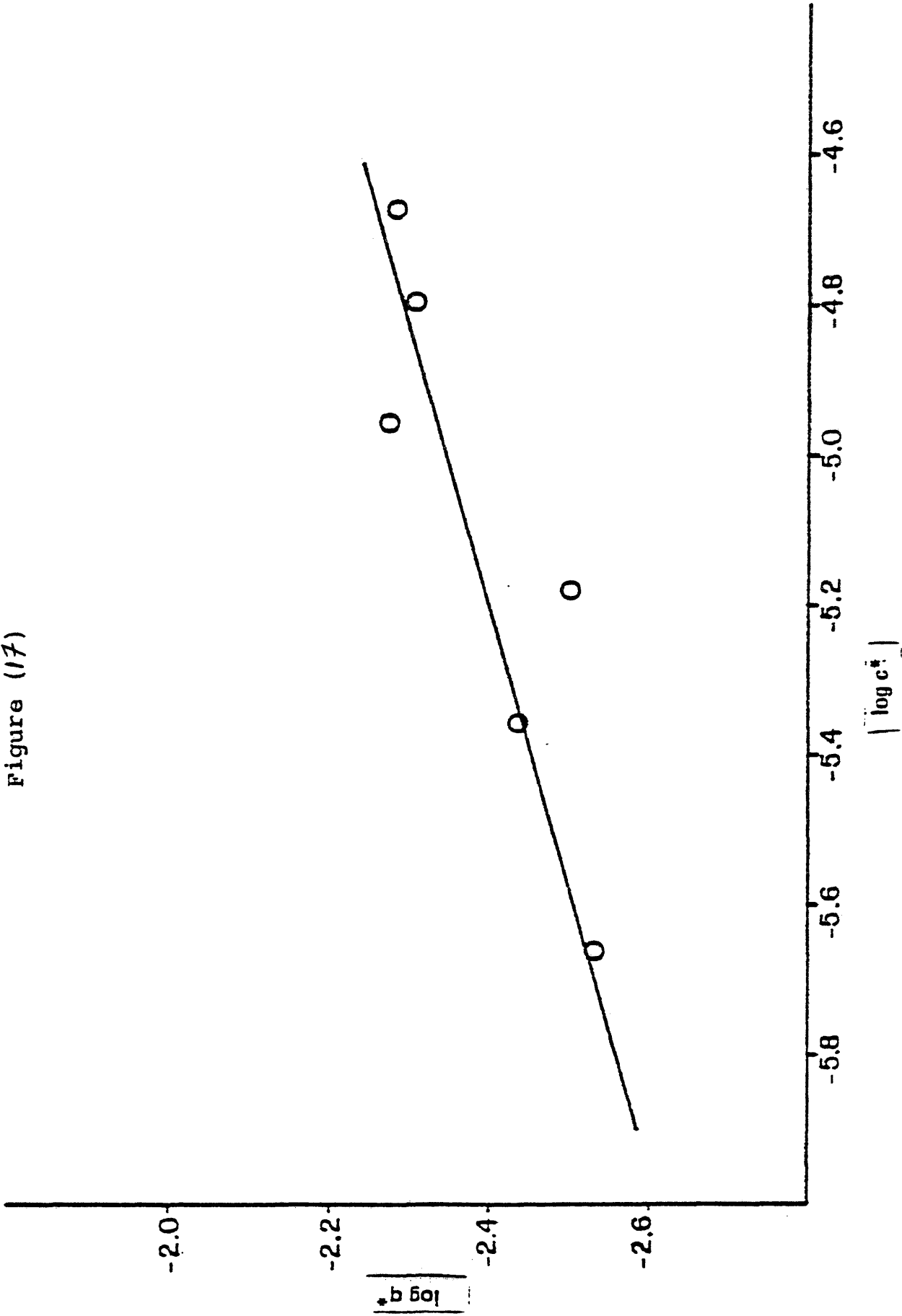
Least Square Fit for Freundlich Model at 10°C

Figure (16)



Least Square Fit for Freundlich Model at $T = 27^{\circ}\text{C}$

Figure (17)



Least Square Fit for Freundlich Model at T = 40°C

Figure (18)

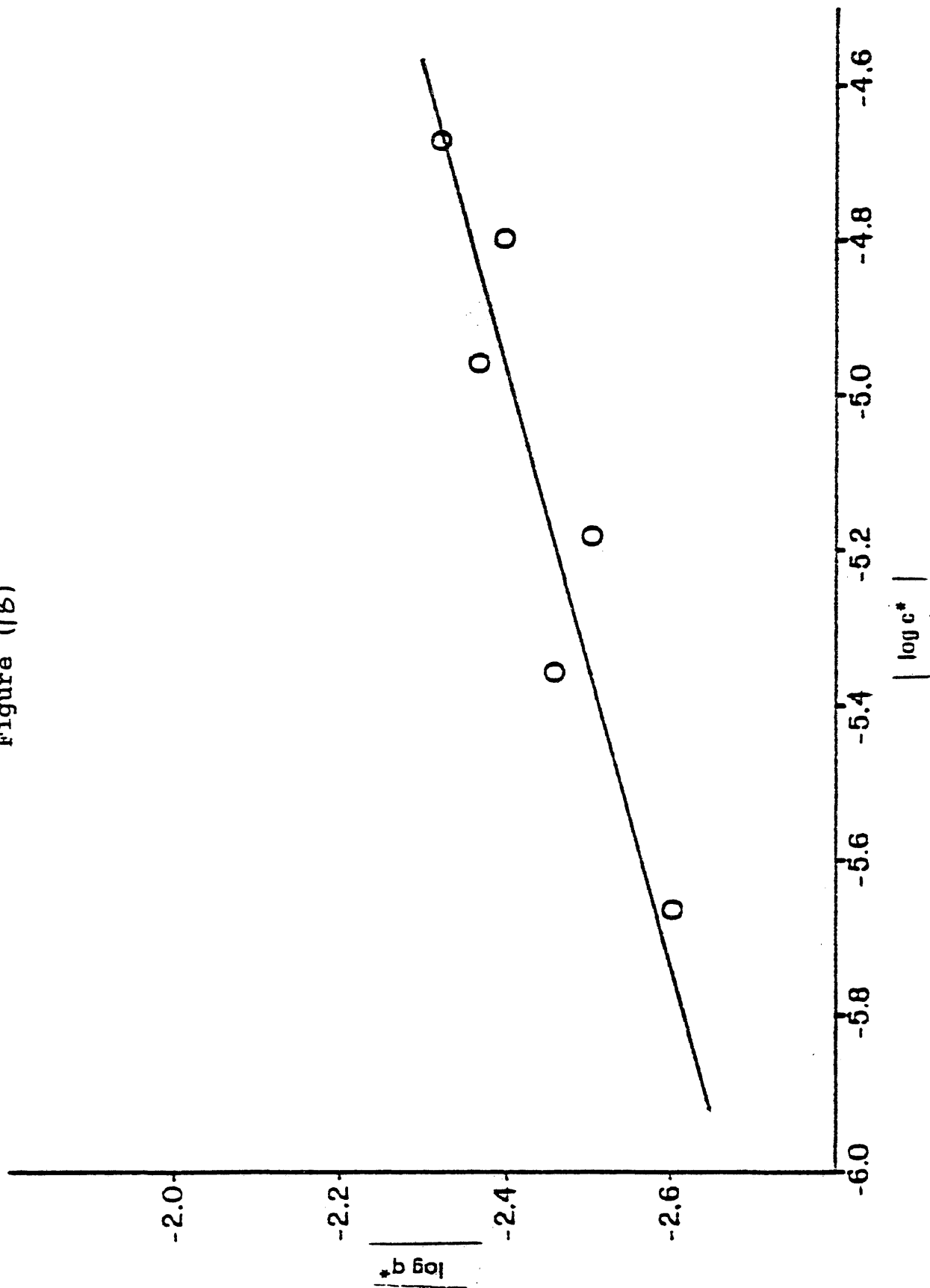


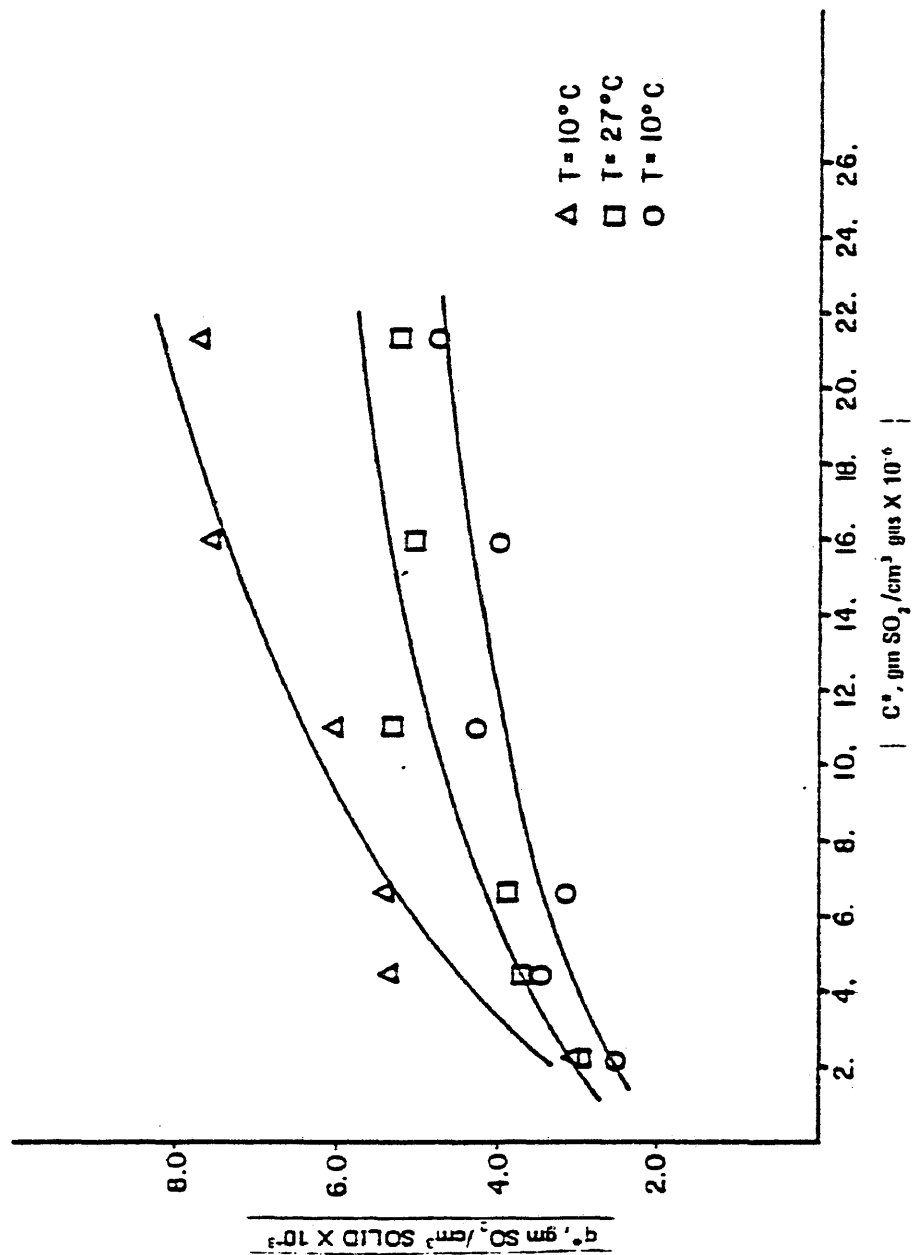
TABLE X
Equilibrium Isotherm Data and Freundlich Constants
for SO₂ on Spent Shale

, $\frac{\text{gm SO}_2}{\text{cm}^3 \text{ gas}} \times 10^{-6}$	q^ , mgm SO ₂ /cm ³ solid		
	T = 10°C	T = 27°C	T = 40°C
2.1866	3.0496	2.9350	2.5090
4.4018	5.3314	3.6609	3.4792
6.6038	5.3990	3.8920	3.1537
11.0056	6.0179	5.3093	4.2897
15.9117	7.5894	5.0032	4.0164
21.8682	7.7693	5.2481	4.7700

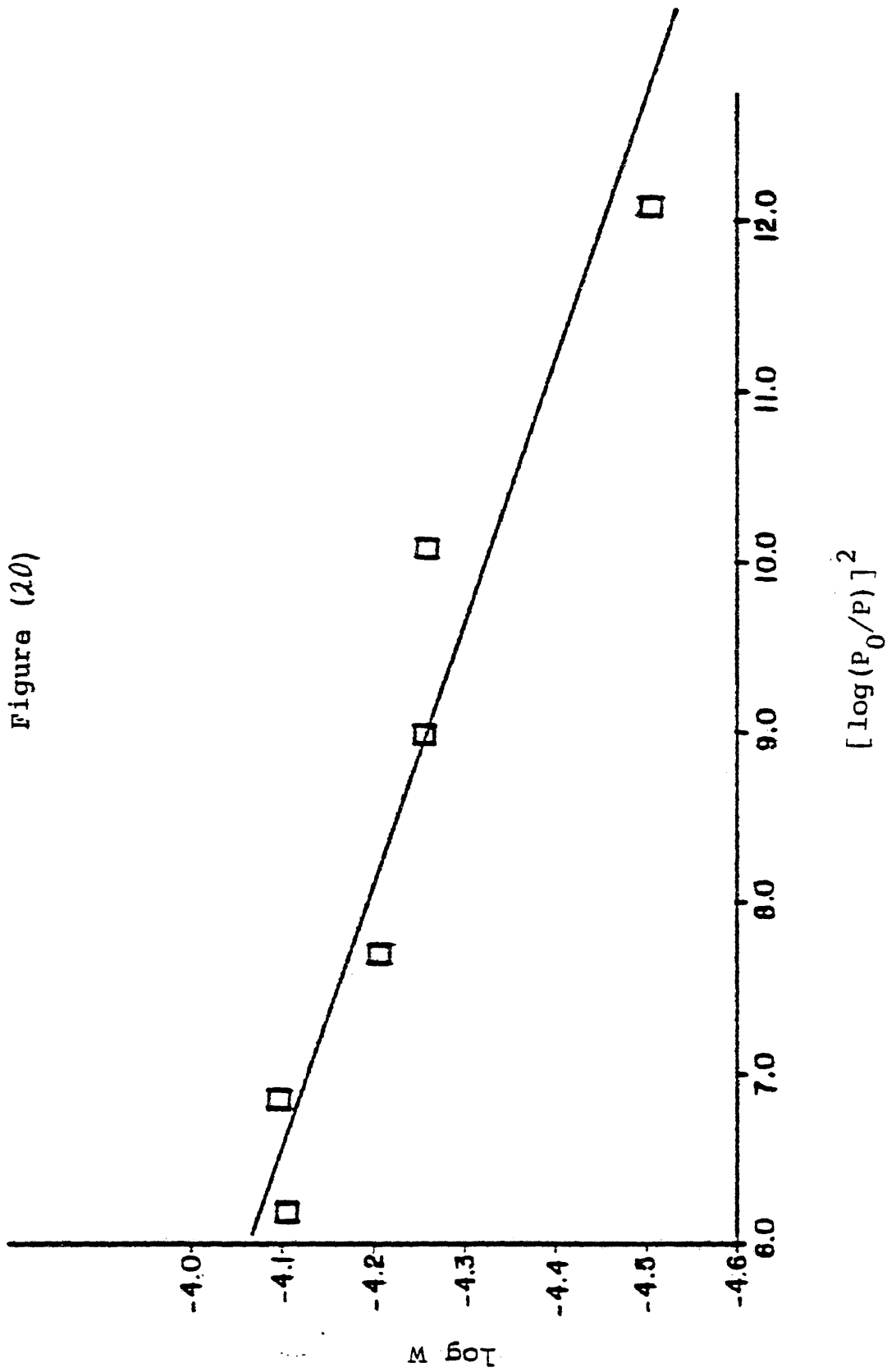
<u>Temperature, °C</u>	<u>K</u>	<u>1/n</u>
10	496.3011 x 10 ⁻³	381.44 x 10 ⁻³
27	105.2423 x 10 ⁻³	270.20 x 10 ⁻³
40	72.6734 x 10 ⁻³	255.15 x 10 ⁻³

Equilibrium Data Fit to Freundlich Model

Figure (19)

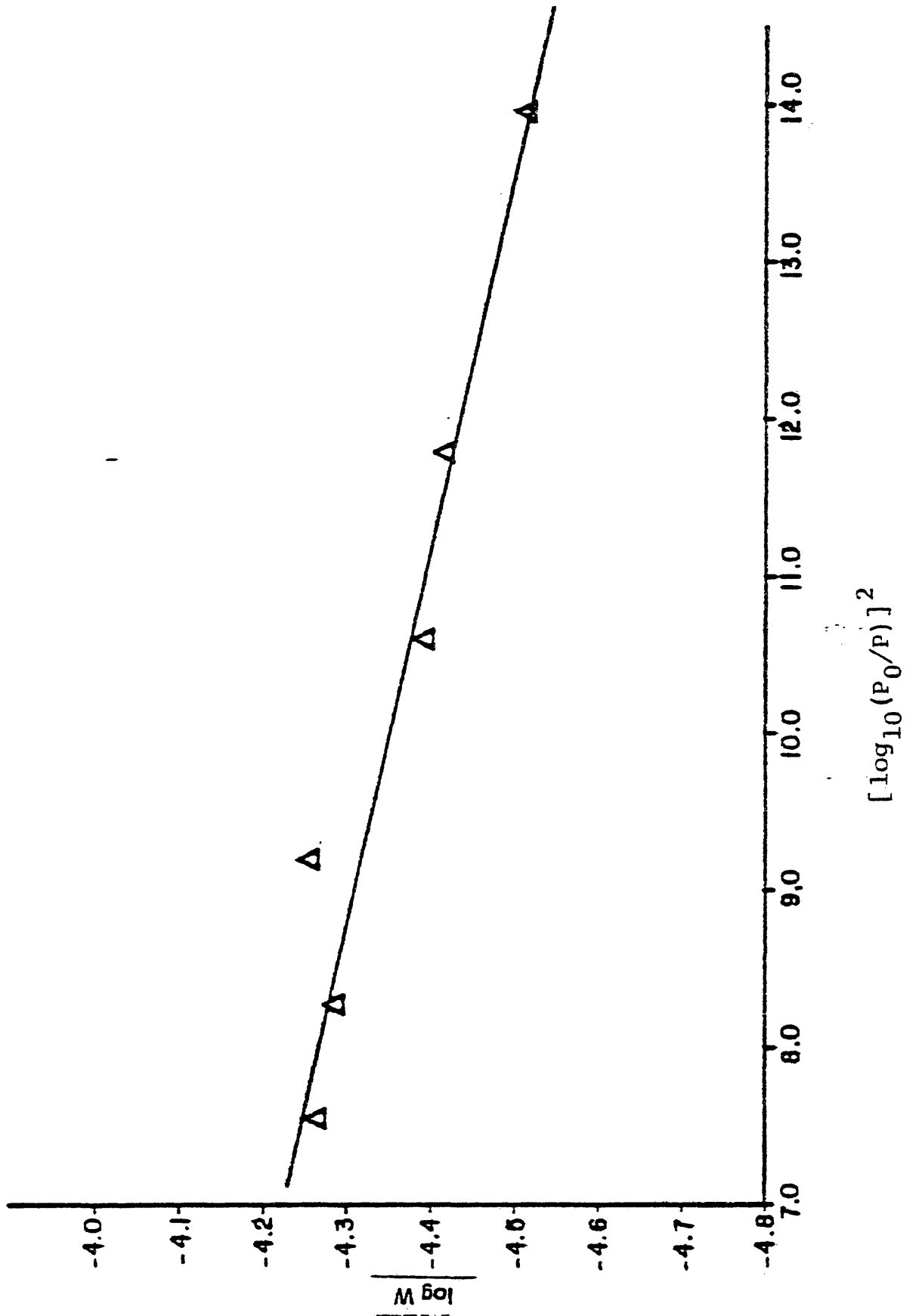


Least Square Fit for Dubinin Model at 10°C



Least Square Fit for Dubinin Model at 27°C

Figure (21)



Least Square Fit for Dubinin Model at 40°C

Figure (21)

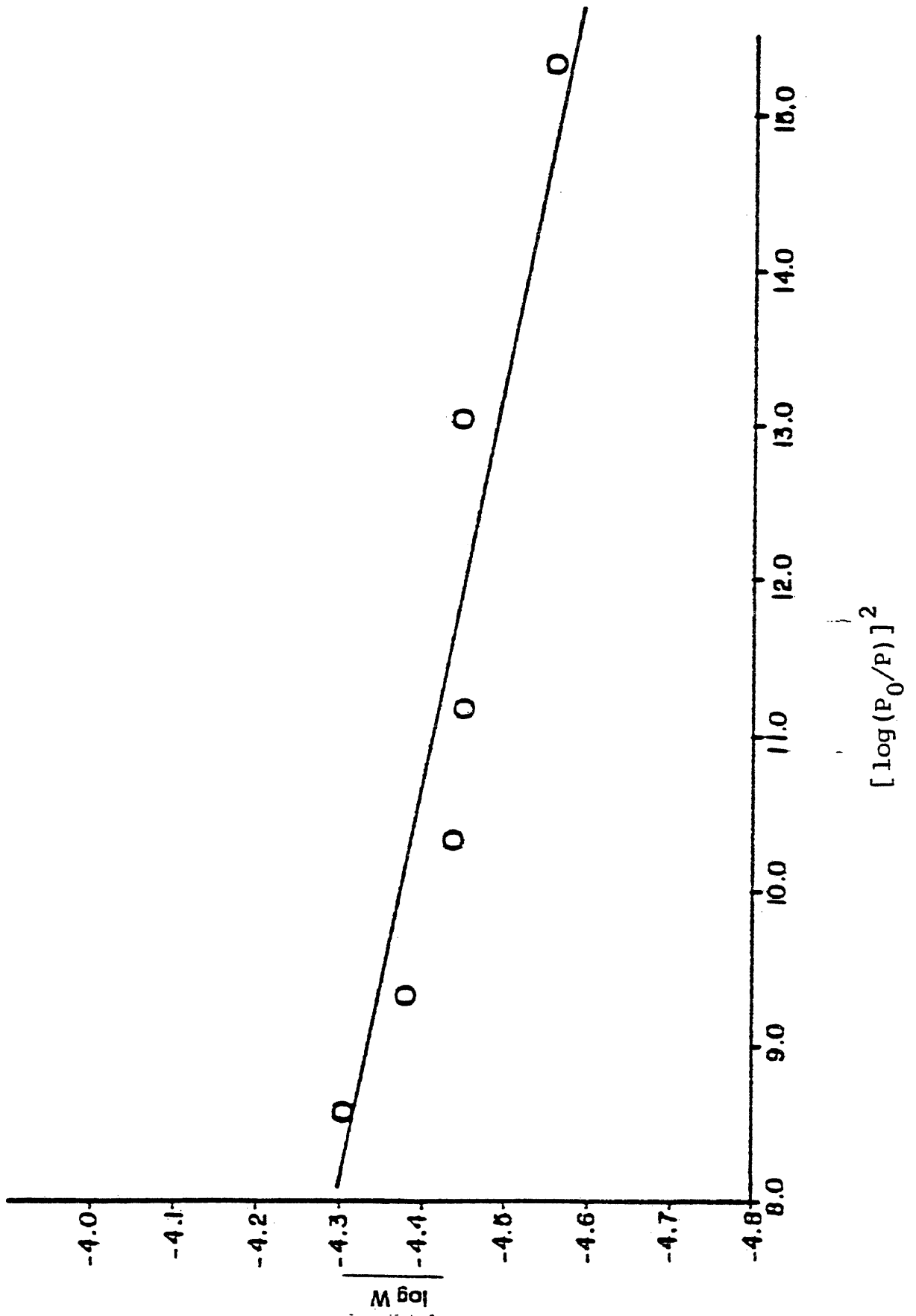


TABLE XI

Equilibrium Isotherm Data and Dubinin Constants
for SO₂ on Spent Shale

<u>Temperature, °C</u>	<u>[log₁₀ (P_c/P)]²</u>	<u>log W, $\frac{\text{moles SO}_2}{\text{gm solid}}$</u>
10	12.09	-4.502
	10.07	-4.259
	8.983	-4.2534
	7.702	-4.2070
	6.839	-4.0930
	6.186	-4.1070
27	13.96	-4.520
	11.78	-4.422
	10.60	-4.396
	9.20	-4.261
	8.25	-4.287
	7.54	-4.266
40	15.33	-4.584
	13.05	-4.442
	11.81	-4.485
	10.34	-4.352
	9.33	-4.380
	8.57	-4.305
<u>Temperatures, °C</u>	<u>W₀</u>	<u>B</u>
10	2.0432 × 10 ⁻⁴	-0.0643
27	1.1790 × 10 ⁻⁴	-0.0421
40	1.0044 × 10 ⁻⁴	-0.0374

The equilibrium data were plotted as W vs $\frac{\Delta G}{R}$ to fit Polanyi's relationship. The value of $\frac{\Delta G}{R}$ is calculated from

$$-\left(\frac{\Delta G}{R}\right) = T * \ln\left(\frac{P_0}{P}\right) \quad \text{Eq. (35)}$$

where T is degrees °K

P_0 = saturation pressure of SO_2 at T&P

P = equilibrium partial pressure

The equilibrium data is given in table XII and the curve fit for this relation is shown in figure 23.

Heat of adsorption

Due to the scatter in uptake data in the low concentration region difficulties were encountered in calculating an accurate value of the heat of adsorption at different loadings. At a loading of 3.5×10^{-3} gm SO_2/cm^3 solid, where less scatter in equilibrium data was noted, the heat of adsorption was obtained. This was done by fitting the data points obtained at the selected loading with a least square regression. The slope was then obtained and the heat of adsorption was calculated and found to be

$$\Delta H = 4.918 \text{ Kcal/gm mole.} \quad \text{Eq. (36)}$$

The least square fit is shown in figure 24.

Intraparticle diffusion coefficients

The theoretical breakthrough curves used in this study were obtained using a computer program which duplicates Antonson's results. Because of the highly nonlinear isotherms exhibited by the adsorption of SO_2 on spent shale, the computer generated breakthrough curves of this work were not in the same range as Antonson's. The intraparticle diffusion coefficients were obtained by curve fitting the experimental

TABLE XII

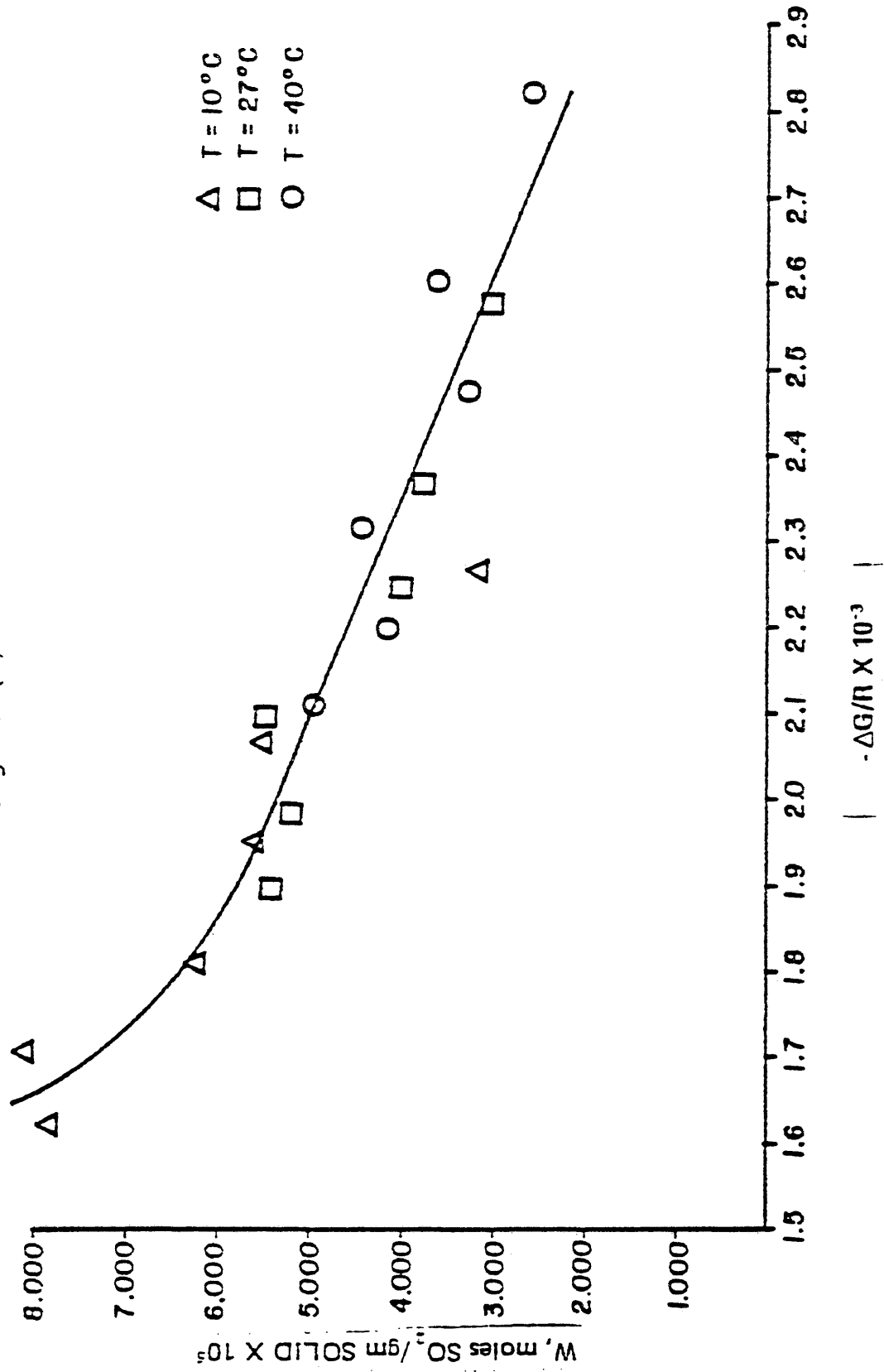
Equilibrium Isotherm Data to Fit Polanyi Equation

SO₂ on Spent Shale

<u>Temperature, °C</u>	<u>W, moles SO₂/gm solid</u>	<u>-ΔG/R</u>
10	3.151 x 10 ⁻⁵	2265.8
	5.508 x 10 ⁻⁵	2067.79
	5.580 x 10 ⁻⁵	1953.00
	6.216 x 10 ⁻⁵	1808.46
	8.081 x 10 ⁻⁵	1704.13
	7.815 x 10 ⁻⁵	1620.69
27	3.032 x 10 ⁻⁵	2580.47
	3.782 x 10 ⁻⁵	2370.57
	4.021 x 10 ⁻⁵	2248.88
	5.485 x 10 ⁻⁵	2095.65
	5.169 x 10 ⁻⁵	1985.06
	5.422 x 10 ⁻⁵	1896.60
40	2.604 x 10 ⁻⁵	2822.85
	3.610 x 10 ⁻⁵	2603.86
	3.272 x 10 ⁻⁵	2476.89
	4.451 x 10 ⁻⁵	2317.03
	4.168 x 10 ⁻⁵	2201.64
	4.950 x 10 ⁻⁵	2109.35

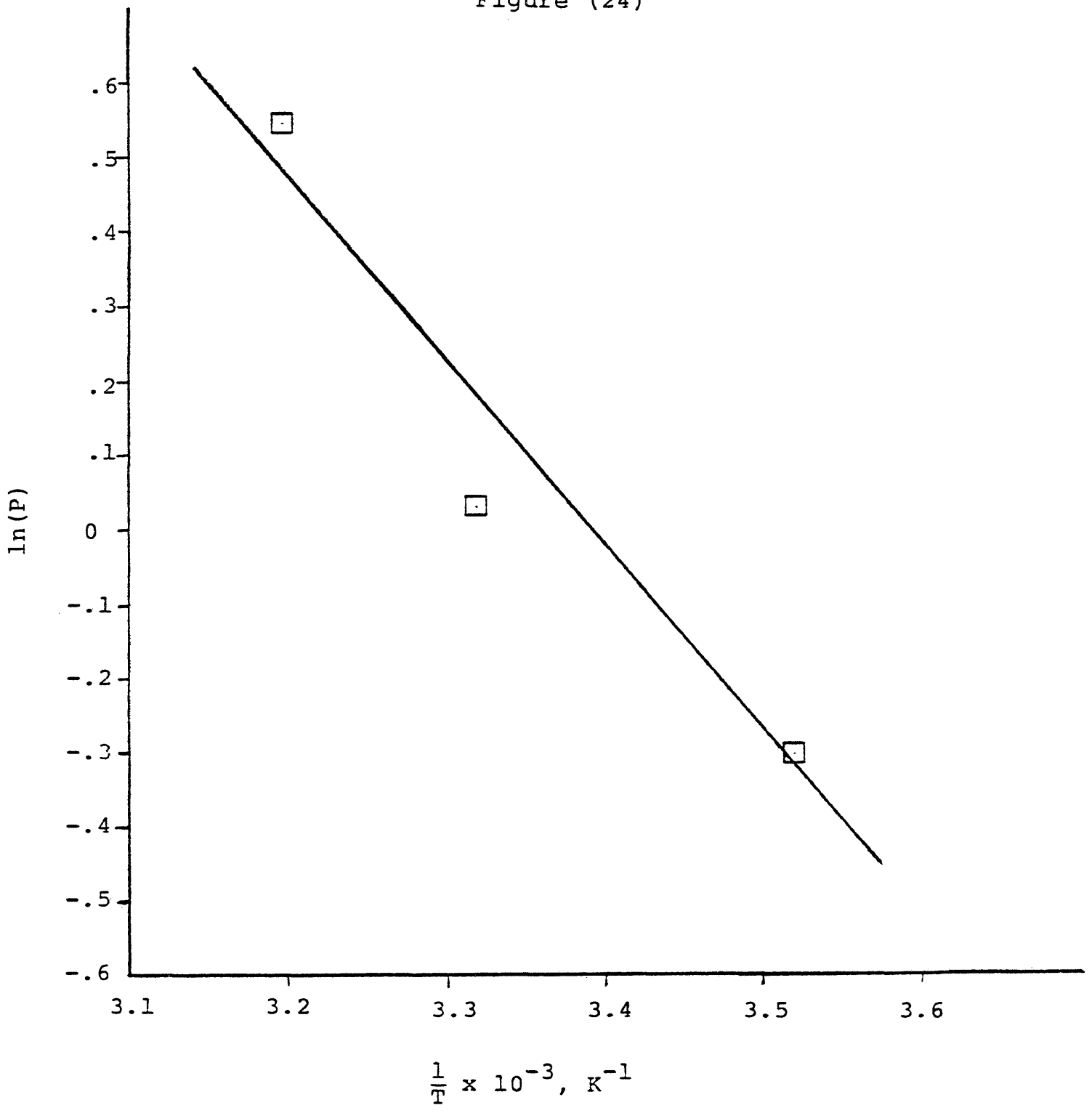
Polanyi Model

Figure (23)



Equilibrium Isotherm for SO₂ Sorption of Spent Shale

Figure (24)



data to the theoretical breakthrough curves to obtain a value of η . Diffusion coefficients are then calculated from

$$D = \frac{mVR_1^2}{3az} \eta \quad \text{Eq. (37)}$$

The experimental breakthrough curves are plotted as $\log \theta_T/\eta$ vs C/C_0 in order to match the computer generated breakthrough curves which are also plotted as $\log \theta_T/\eta$ vs C/C_0 . At a fixed value of C/C_0 on the experimental breakthrough curve, the corresponding value of θ was found. θ_T/η was then calculated from

$$\theta_T/\eta = (2mV/3az) \theta \quad \text{Eq. (38)}$$

The bed height, velocity, particle size, and void fraction ratio are all measured. The calculated diffusion coefficients for 10 and 40°C are shown in table XIII. Experimental breakthrough curves are compared to theoretical curves in figures 25, 26, 27, 28, 29 and 30. The variations of diffusion coefficients with adsorbate concentrations are shown in figures 31 and 32.

The difficulties encountered in this trial and error calculation were due to the lack of a large number of computer generated breakthrough curves. Only a selected number of theoretical curves parametric in η could be generated due to the high cost of executing the computer program. The other difficulty encountered was due to the sensitivity of the void volume measurements to the diffusion coefficient calculations.

Void volume of the packed bed was measured by weighing the amount of spent shale used for the adsorption study. The error

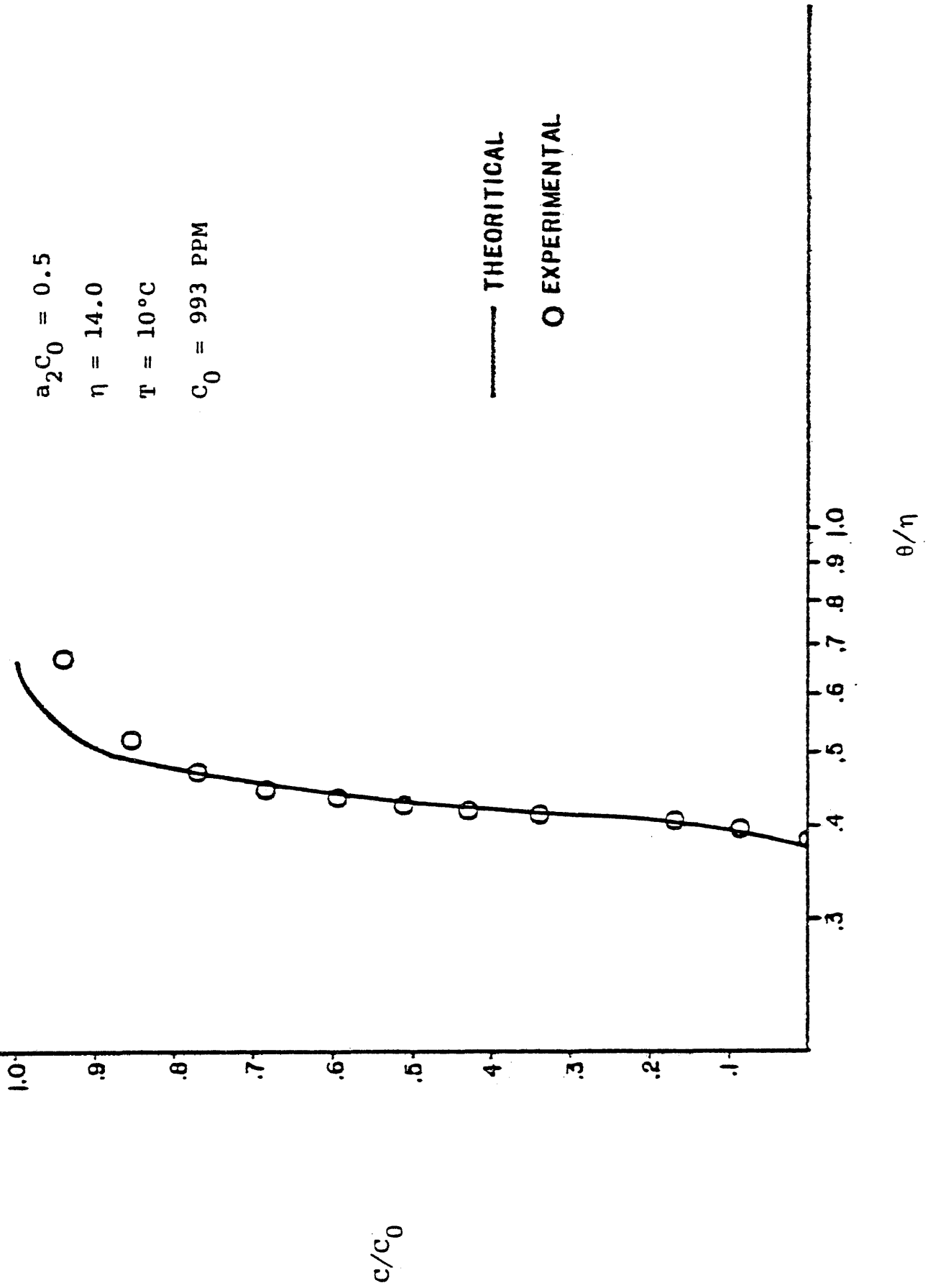
TABLE XIII

Diffusion coefficients calculated from
the Adsorption of SO₂ on Spent Shale

<u>Temperature, °C</u>	<u>Adsorbent concentration, PPM SO₂ in nitrogen</u>	<u>D (cm²/sec) x 10⁵</u>
10	993	2.91
	2,998	3.46
	4,998	3.74
40	993	3.23
	2,99	5.49
	4,998	6.098

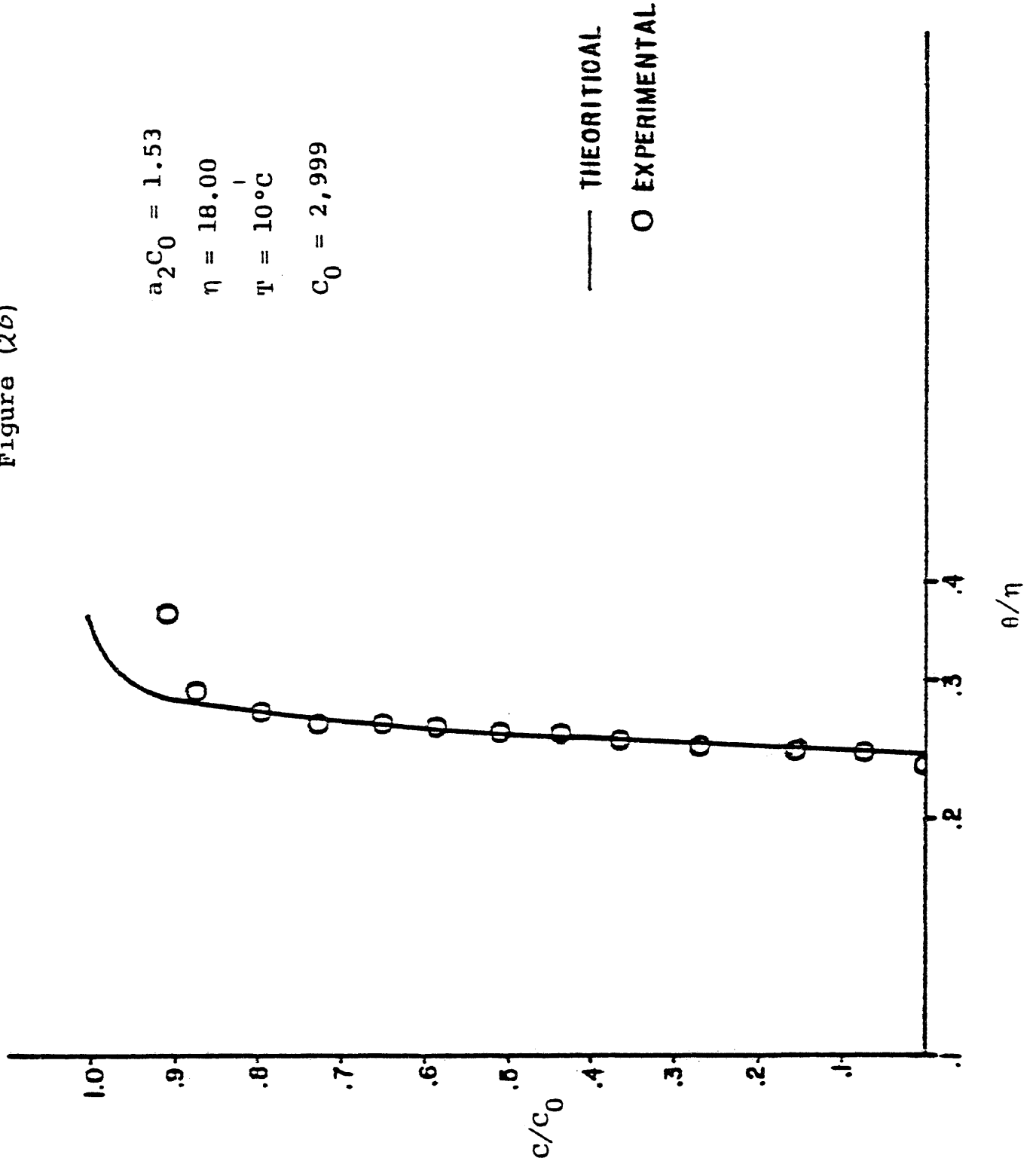
Curve Fit for $\eta = 14.0$

Figure (15)



Curve Fit for $\eta = 18.00$

Figure (26)



Curve Fit for $\eta = 18.0$

Figure (27)

$$a_2 C_0 = 2.55$$

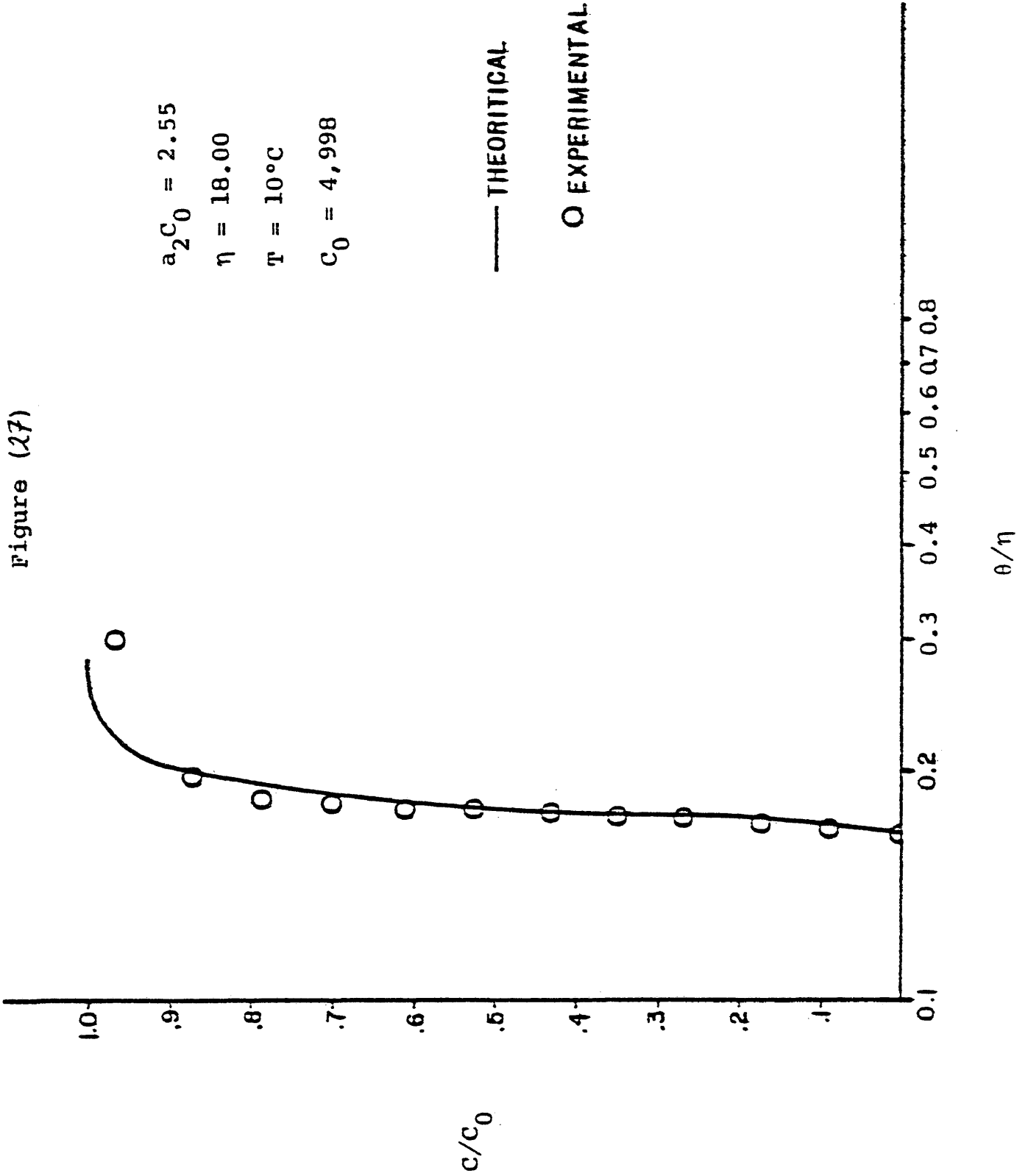
$$\eta = 18.00$$

$$T = 10^\circ\text{C}$$

$$C_0 = 4,998$$

— THEORETICAL

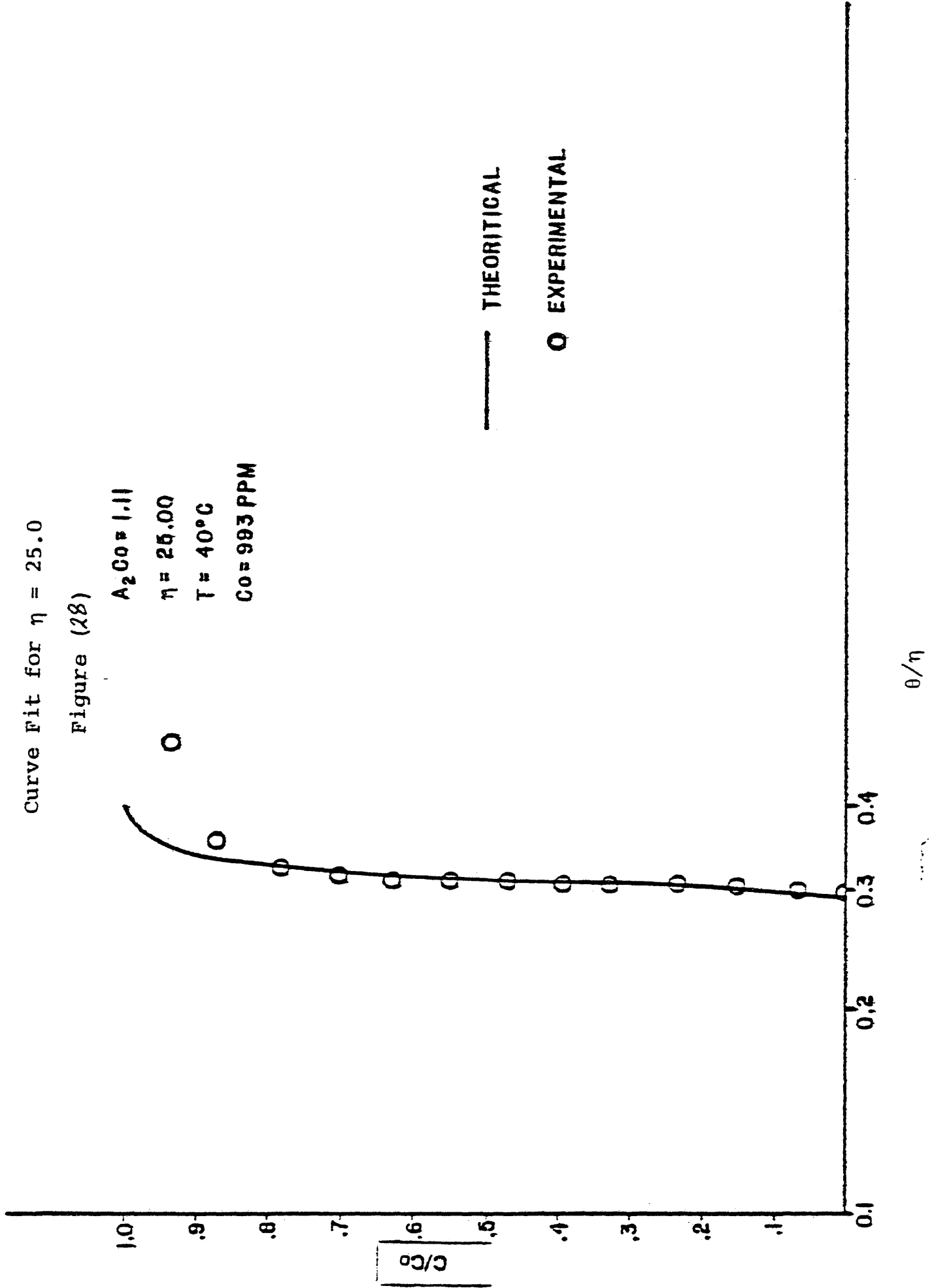
O EXPERIMENTAL



Curve Fit for $\eta = 25.0$

Figure (28)

$A_2Co = 1.11$
 $\eta = 25.00$
 $T = 40^\circ C$
 $Co = 993 PPM$



Curve Fit for $\eta = 35.0$

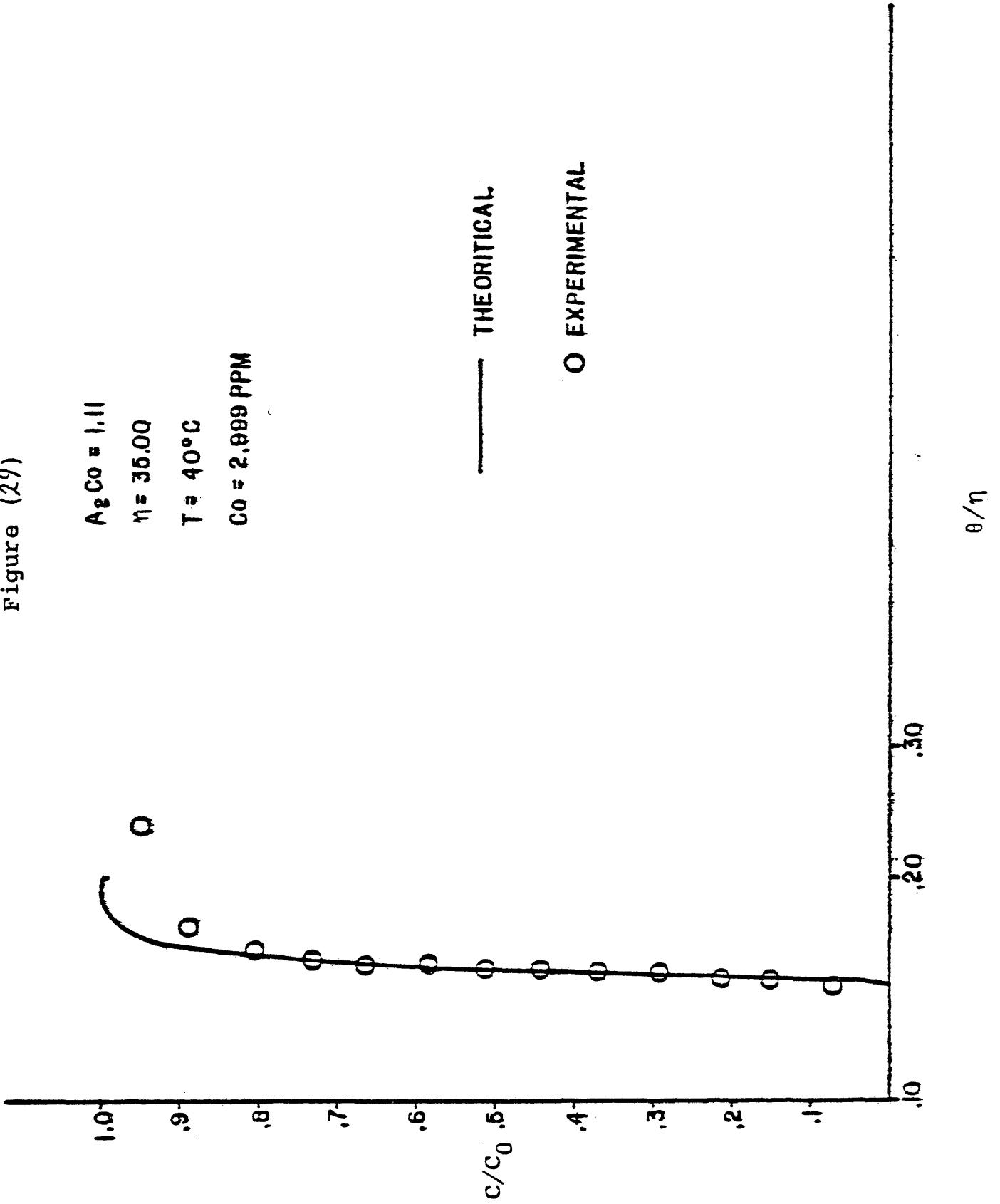
Figure (29)

$A_2 C_0 = 1.11$

$\eta = 35.00$

$T = 40^\circ\text{C}$

$C_0 = 2.999 \text{ PPM}$



θ/η

Curve fit for $\eta = 45$

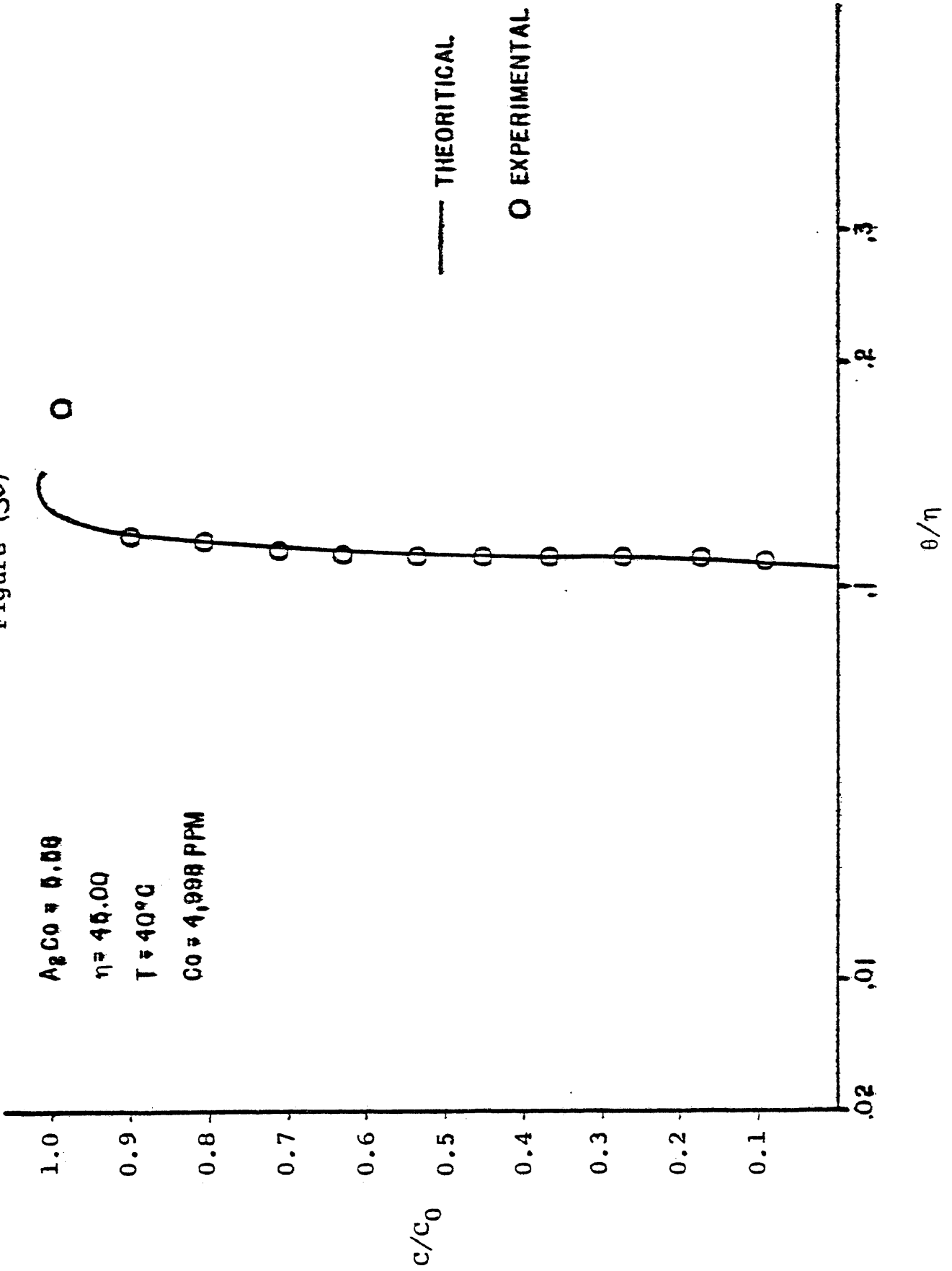
Figure (30)

$A_2CO = 0.08$

$\eta = 45.00$

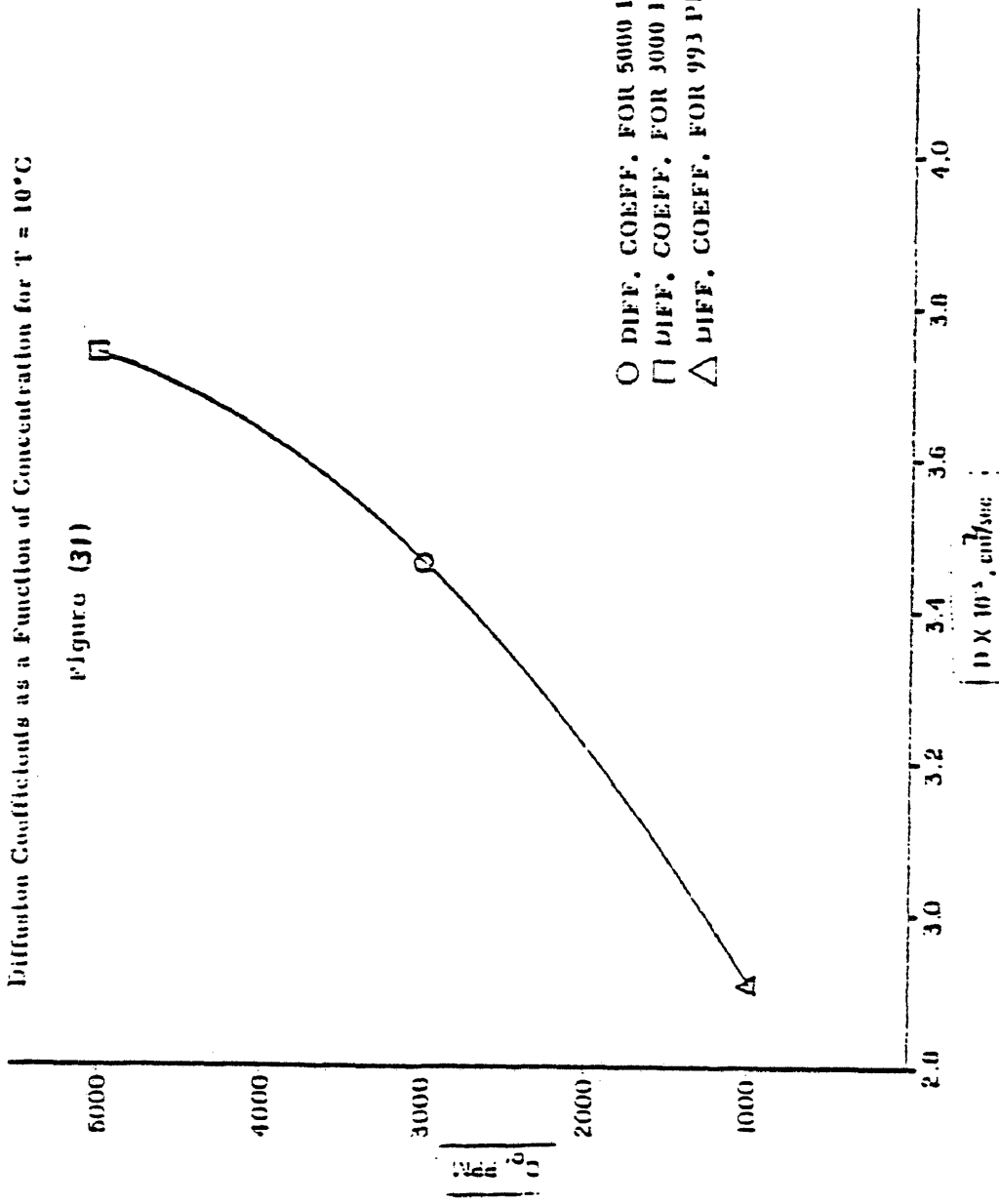
$T = 40^\circ C$

$CO = 1,998 \text{ PPM}$



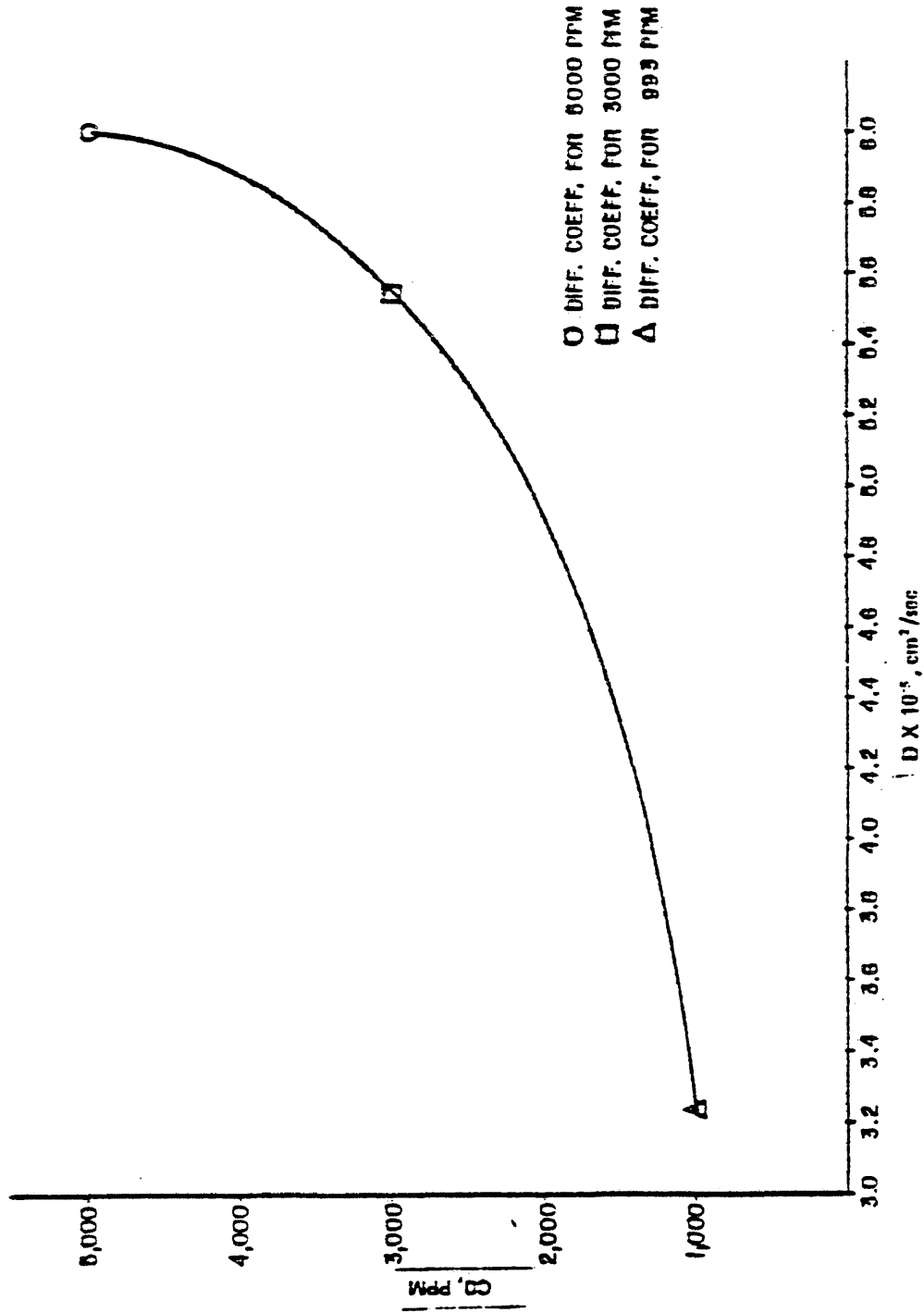
Diffusion Coefficients as a Function of Concentration for T = 10°C

Figure (31)



○ DIFF. COEFF. FOR 5000 PPM
□ DIFF. COEFF. FOR 3000 PPM
Δ DIFF. COEFF. FOR 993 PPM

Diffusion Coefficients as a Function of Concentration at T = 40°C
Figure (3λ)



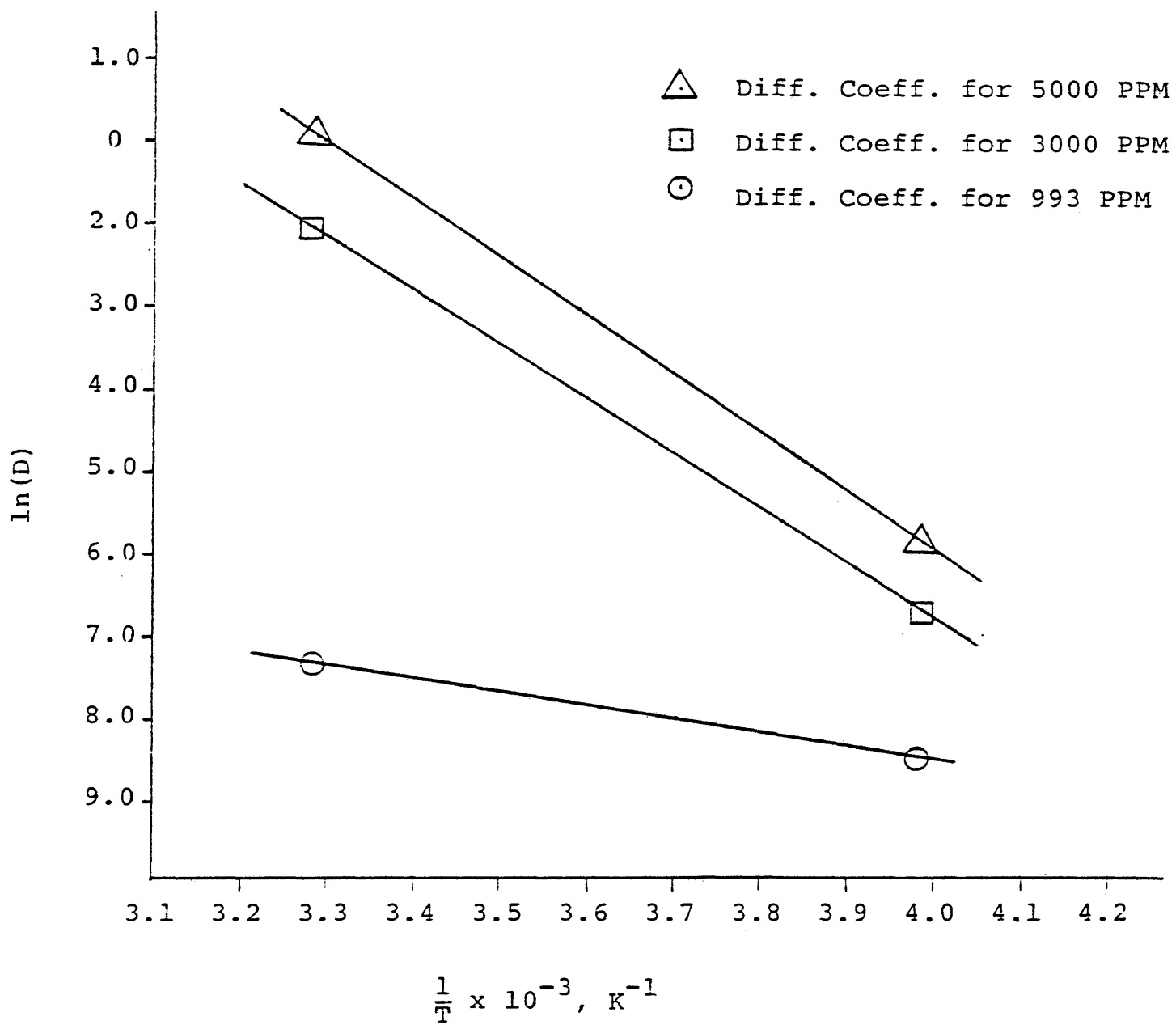
encountered in this measurement was due to the non-uniform bed density. It was necessary to curve match the experimental data and then back out the exact value of the void volume before the final curve match was done. It was also necessary to interpolate between the computer generated breakthrough curves to find the best value of η .

Finally, the calculated diffusivities were used to estimate the activation energy. This was done by plotting $\ln(D)$ vs the inverse of the bath temperature as shown in figure 33. The least squares line through the data yielded the Arrhenius coefficients D_0 and $(-E_a)$ in the relation

$$D = D_0 \exp(-E_a/RT) \quad \text{Eq. (39)}$$

The Arrhenius coefficients are given below at three different concentrations

C_0 , PPM SO_2 in N_2	D_0 , cm^2/sec	E_a/R
993	3.33651×10^{-5}	-156.85
2,998	6.25215×10^{-5}	-672.71
4,998	7.02114×10^{-5}	-707.93



CONCLUSION AND RECOMMENDATIONS

The most apparent conclusion that can be drawn from this experiment is the adsorptive properties of spent shale that was retorted at different temperatures. The spent shale sample that was retorted at 700°C showed a maximum surface area which resulted in a maximum adsorption of SO₂. The results of this investigation also offer an attractive method of utilizing waste materials which result from above ground retorting of oil shale. In this practice, sulfur dioxide which is considered to be one of the largest air pollutants in industry, can be removed from the gas streams at a low operating cost as well as low capital investment. The other attractive method for disposing of waste gases can be effectively done by the introduction of combustion gases into the underground formation where in situ processing has occurred.

A desorption curve, which was obtained for some of the runs by passing pure nitrogen at 27°C through the packed bed, showed that only approximately 90% of the sulfur dioxide was recovered. This indicated that some chemisorption may have occurred in conjunction with the physical adsorption.

Although the equilibrium uptake of SO₂ on spent shale is low compared to activated carbon, the lack of SO₂ given off from the controlled state retort in Laramie, Wyoming can indeed be attributed to its adsorption on spent shale. From the curve fit of the experimental data, the Langmuir equilibrium isotherm

was the most reasonable representation of the equilibrium uptake of SO_2 on spent shale.

The capacity of spent shale and the increased breakthrough time were obtained as a result of decrease in bath temperature.

Diffusion coefficients calculated in this study using a Langmuir type isotherm, which fit the experimental data very well, were believed to be quite accurate.

The calculated value of the heat of adsorption is of the same order of magnitude as that of the heat of condensation which justify for the physical adsorption property.

The activation energy increases as the adsorbate concentration increases due to the diffusion coefficient's dependency on concentration.

Further study of the temperature effects of diffusion coefficients are recommended in order to calculate a more accurate value of the activation energy.

NOMENCLATURE

- a = external mass transfer area
 a' = constant
 a_1 = Langmuir constant, dimensionless
 a_2 = Langmuir constant, $\text{cm}^3 \text{solid}/\text{gm SO}_2$
 B = slope of Dubinin log-log plot
 C_0 = inlet SO_2 concentration, PPM
 C^* = SO_2 concentration in equilibrium with solid, $\text{gm SO}_2/\text{cm}^3 \text{gas}$
 D = intraparticle diffusion coefficient, cm^2/sec
 D_i = inside diameter, cm
 D_0 = intercept of Arrhenius plot (cm^2/sec)
 E_a = slope of Arrhenius plot
 K = constant for Freundlich, dimensionless
 K_D = equilibrium distribution coefficient for Rosen's linear isotherm model
 K_L = external mass transfer coefficient
 m = void volume per unit volume of adsorbent
 q^* = overall concentration of adsorbed SO_2 per unit mass of adsorbent, $\text{mg SO}_2/\text{cm}^3 \text{solid}$
 q_i = point concentration of SO_2 within adsorbent, $\text{mg SO}_2/\text{cm}^3 \text{solid}$
 q_s = surface SO_2 concentration, $\text{mg SO}_2/\text{cm}^3 \text{solid}$
 R = particle radius, cm
 r = radial distance from center of particle
 R_f = film type resistance for Rosen's model
 t = time, min
 V = linear flow velocity (V_0/ϵ) cm/sec

$X = Z/mV$, time required for fluid to flow a distance Z/m

$W =$ volume of adsorbed molecules, cm^3/gm

$Z =$ bed height measured from column inlet

Greek letters

$\beta =$ affinity coefficient (moles/cal)

$\epsilon =$ bed void volume

$\lambda =$ dummy variable of integration

$\theta = t - Z/mV$, time measured after contact by fluid, min

$\theta_T = \frac{2D}{R^2} \theta$, dimensionless

$\mu_2 =$ chemical potential sorbate

$\mu_1 =$ chemical potential of saturated liquid

$\eta = (3Da_2/R^2)X$, effective bed length, dimensionless

$\phi = C/C_0$, normalized concentration

$\rho_B =$ bed bulk density, gm/cm^2

$\rho_L =$ liquid density, gm/cm^3

$\sigma_n = n\pi/R$

$\Delta G =$ adsorption potential (cal/mole)

REFERENCES

1. Acrivos, A., Chem. Eng. Sci., 13, 1, 1960.
2. Antonson, C. R. and Dranoff, J. S., "Kinetics of ethane adsorption on molecular sieves," CEP Symp. Series, 63, (74), p. 61.
3. Antonson, C. R., "Kinetics of Ethane adsorption on molecular sieves," Masters Thesis, Evanston, Ill., Northwestern U., 1966.
4. Antonson, C. R., "Adsorption of Ethane in Molecular sieve particles," PhD Dissertation, Evanston, Ill., Northwestern U., 1968.
5. Collins, J. J., "The lub/equilibrium section concept for fixed-bed adsorption," CEP Symp. Series, 63, (84), p. 31.
6. Cooney, D. O., and Lightfoot, E. N., "Existence of asymptotic solutions to fixed-bed separations and exchange equations," I and EC Fund., 4, (2), p. 233, 1965.
7. Culbertson, W. J., Jr., Nevens, T. D., and Hollingshead, R. D., "Disposal of oil shale ash," Colo. School Mines Quart., 65, (4), 89, 1970.
8. Davis, T. J., "Mass-transfer and interfacial phenomena," Advances in Chemical Engineering, IV, Academic Press, Inc., New York, 1958, Editors T. B. Drew and J. W. Hooper, p. 147.
9. Dubinin, M. M., Proc. Conf. Ind. Carb. Graph., SCI, p. 219, 1958.
10. Dubinin, M. M., Russ. J. Phys. Chem., (Eng. Trans.), 697, 1965.

11. Eagleton, L. C. and Bliss, H., "Drying of Air in Fixed B Beds," CEP, 49, (10), p. 543, 1953.
12. Engineering Science, Inc., "Air quality assessment of the oil shale development program in the Piceance Creek Basin," Federal Energy Adm. Proj. Independence Blueprint, potential future role of oil shale, prospects and constraints, p. 390, Nov. 1974.
13. Gupta, J. C., Yi Hua Ma and Sand, L. B., "Diffusion of sulfur dioxide in a synthetic mordenite and a natural erionite," AIChE Symp. Series, 67, (117), p. 51, 1971
14. Hall, K. R., Eagleton, L. C., Acrivos, A., and Vermuellen, T., "Pore and solid diffusion kinetics in fixed bed adsorption under constant pattern conditions," I and EC Fund., 5, (2), p. 212, 1966.
15. Hasanain, M. A., A. L. Hines, C. L. Murphy, and J. J. Duvall, "Adsorption of SO₂ on spent shale in packed beds," Proc. 2nd Pacific Chem. Eng. Congr. (Pachec 77), Denver, 1977.
16. Hatfield, J. A., C. L. Murphy, and A. L. Hines, "Adsorption of SO₂ on peanut hulls," Proc. 3rd Natl. Conf. on Complete Waste Reuse, 212-216, Cincinnati, 1976.
17. Hersh, C. K., Molecular Sieves, Reinhold, New York, 1961.
18. Hines, A. L., Class notes for CR 615, Colo. School Mines, Spring, 1977.
19. Hines, A. L., Personal communication, May 6, 1976.
20. Jukkola, E. E., A. J. Denilauler, H. B. Jensen, W. I. Barnett, and W. I. Murphy, Ind. Eng. Chem., 45, 2711, 1953.

21. Kidnay, A. J. and M. J. Hiza, "The purification of Helium-Gas by physical adsorption at 76°K," AICHE J., 16, (6), p. 949, 1970.
22. Kondis, F. E. and J. S. Dranoff, "Nonisothermal sorption of ethane by molecular sieves," AICHE Symp. Series, 67, (117), p. 25, 1971.
23. Mesamune, S. and J. M. Smith, "Adsorption rate studies significance of pore diffusion," AICHE J., 10, (2), p. 24, 1964.
24. Murphy, C. L., "Adsorption of ionic mercury in aqueous solution by waste rubber in packed beds," Masters thesis, Colo. School Mines, 1977.
25. Polanyi, M., Verh. Itsh. physik Ges., 16, 1012, 1914.
26. Rimple, A. E., D. T. Camp, J. A. Kostecky, and L. N. Canjar, "Kinetics of physical adsorption of propane from helium on fixed beds of activated alumina," CEP Symp. Series, 63, (74), p. 53.
27. Rosen, J. B., "General Numerical solution for solid diffusion in fixed beds," I and EC, 46, (8), p. 1590, 1954.
28. Rosen, J. B., "Kinetics of a fixed bed system for solid diffusion into spherical particles," J. Chem. Phys., 20, (3), p. 387, 1952.
29. Ruthven, D. M. and K. F. Laughlin, "Diffusion in molecular sieves," AICHE Series, 67, (117), p. 35, 1971.
30. Smith, F. B. and G. Burnet, "Dynamic Exchange adsorption of propane-propylene on activated carbon," AICHE Symp Series, 67, (117), p. 58, 1971.

31. Smith, J. M., Chemical Engineering Kinetics, 2nd Ed., McGraw-Hill, 1970.
32. Smith, J. W., "Thermal analysis in earth science: experience and expectations," Thermal Analysis, 3, Proc. 3rd ICTA DAVOS, p. 605-635, 1971.
33. Striffler, W. D., I. F. Wymore and W. A. Berg, "Characteristics of spent shale which influence water quality, sedimentation and plant growth medium," Colo. State U., Tech. Rept., Surface rehabilitation of land disturbances resulting from oil shale development, March 1974.
34. Stuart, F. X., and D. T. Camp, "Comparison of Kinetic and diffusional models for packed bed adsorption," I and EC Fund., 6, (1), p. 156, 1967.
35. Testin, R. F. and E. B. Stuart, "Diffusion coefficients measured from gas-solid adsorption rate experiments," AIChE Series, 63, (74), p. 10, 1971.
36. Treybal, R. E., Mass Transfer Operations, 2nd Ed., McGraw-Hill, 1968.
37. Vermuellen, T., "Theory for irreversible and constant pattern diffusion," I and EC, 45, (8), 1664, 1953.
38. Vermuellen, T., "Separation by adsorption methods," Adv. Chem. Eng., II, Academic Press, Inc., New York, 1958, Editors T. B. Drew and J. W. Hooper, p. 147, 1958.
39. Weber, W. J. and R. R. Rumer, "Intraparticle transport of sulfonated alkylbenzene in a porous solid: Diffusion with nonlinear adsorption," Water Res., 1, (3), p. 361, 1965.

APPENDIX A
Experimental Data

Adsorption Gas Concentration <u>993</u> PPM		Adsorption Gas Concentration <u>1998</u> PPM	
Temperature 10°C		Temperature 10°C	
Time/unit wt., min/gm	c/c ₀	Time/unit wt., min/gm	c/c ₀
10.73	0.000	10.83	0.000
11.08	0.086	11.03	0.098
11.25	0.171	11.10	0.195
11.42	0.257	11.17	0.293
11.56	0.342	11.25	0.390
11.73	0.428	11.31	0.488
11.90	0.513	11.39	0.586
12.13	0.598	11.47	0.683
12.48	0.684	11.67	0.780
13.17	0.770	12.69	0.878
14.53	0.855	24.52	0.975
18.52	0.940	31.42	1.000
27.10	1.000		

Adsorption Gas Concentration <u>2998</u> PPM		Adsorption Gas Concentration <u>4998</u> PPM	
Temperature 10°C		Temperature 10°C	
time/unit wt., min/gm	c/c ₀	time/unit wt., min/gm	c/c ₀
7.04	0.000	4.54	0.000
7.31	0.072	4.69	0.038
7.43	0.144	4.76	0.175
7.53	0.266	4.81	0.263
7.62	0.291	4.86	0.350
7.69	0.363	4.91	0.438
7.75	0.436	4.96	0.526
7.80	0.508	5.01	0.613
7.85	0.581	5.05	0.701
7.90	0.653	5.12	0.788
7.95	0.726	5.46	0.876
8.17	0.799	8.31	0.964
8.71	0.875	21.27	1.000
11.01	0.910		
19.88	1.000		

Adsorption Gas Concentration <u>7226</u> PPM		Adsorption Gas Concentration <u>9704</u> PPM	
Temperature 10°C		Temperature 10°C	
Time/unit wt., min/gm	c/c ₀	Time/unit wt., min/gm	c/c ₀
3.80	0.000	2.07	0.000
3.89	0.111	2.15	0.089
3.93	0.166	2.19	0.179
3.97	0.163	2.22	0.270
4.00	0.278	2.25	0.358
4.03	0.331	2.27	0.450
4.05	0.400	2.32	0.537
4.08	0.446	2.38	0.626
4.11	0.582	2.47	0.701
4.14	0.555	2.78	0.740
4.17	0.608	3.55	0.863
4.20	0.665	4.51	0.953
4.23	0.718		
4.27	0.772		
4.34	0.881		
6.89	0.938		
11.04	0.989		
15.29	1.000		

Adsorption Gas Concentration <u>993</u> PPM		Adsorption gas Concentration <u>1999</u> PPM	
Temperature 27°C		Temperature 27°C	
Time/unit wt., min/gm	c/c ₀	Time/unit wt., min/gm	c/c ₀
10.98	0.00	8.40	0.00
11.08	0.50	8.42	0.50
11.19	0.10	8.45	0.10
11.30	0.15	8.58	0.15
11.40	0.20	8.60	0.20
11.48	0.25	8.62	0.25
11.60	0.30	8.71	0.30
11.80	0.35	8.80	0.35
11.98	0.40	8.88	0.40
12.09	0.45	9.00	0.45
12.30	0.50	9.12	0.50
12.48	0.55	9.23	0.55
12.80	0.60	9.42	0.60
13.80	0.70	10.58	0.75
15.80	0.8	11.4	0.80
20.30	0.9	14.4	0.90
28.00	0.950	24.4	1.00

Adsorption Gas Concentration <u>2999</u> PPM		Adsorption Gas Concentration <u>4998</u> PPM	
Temperature 27°C		Temperature 27°C	
Time/unit wt., min/gm	c/c ₀	Time/unit wt., min/gm	c/c ₀
4.15	0.00	3.55	0.00
4.40	0.50	3.60	0.50
4.42	0.10	3.60	0.10
4.45	0.15	3.61	0.15
4.50	0.20	3.61	0.20
4.60	0.25	3.62	0.25
4.61	0.30	3.63	0.30
4.61	0.35	3.65	0.35
4.62	0.40	3.70	0.40
4.70	0.45	3.80	0.45
4.80	0.50	3.81	0.50
4.85	0.55	3.90	0.55
5.00	0.60	4.00	0.60
5.38	0.70	4.38	0.70
5.90	0.80	5.00	0.80
7.60	0.90	6.20	0.90
14.40	1.00	11.81	1.00

Adsorption Gas Concentration <u>7226</u> PPM		Adsorption Gas Concentration <u>9704</u> PPM	
Temperature 27°C		Temperature 27°C	
Time/unit wt., min/gm	c/c ₀	Time/unit wt., min/gm	c/c ₀
2.62	0.00	2.30	0.00
2.65	0.05	2.40	0.05
2.67	0.10	2.42	0.10
2.70	0.15	2.45	0.15
2.70	0.2	2.60	0.20
2.80	0.25	2.60	0.25
2.80	0.30	2.60	0.30
2.82	0.35	2.61	0.35
2.82	0.40	2.62	0.40
2.82	0.45	2.68	0.45
2.83	0.50	2.72	0.50
2.83	0.55	2.80	0.55
2.85	0.60	2.81	0.6
3.0	0.70	3.0	0.7
3.4	0.80	3.30	0.8
4.35	0.9	4.0	0.9
5.12	0.95	4.75	0.95

Adsorption Gas Concentration <u>993</u> PPM		Adsorption Gas Concentration <u>1998</u> PPM	
Temperature 40°C		Temperature 40°C	
Time/unit wt., min/gm	c/c ₀	Time/unit wt., min/gm	c/c ₀
11.66	0.000	8.36	0.000
11.79	0.078	8.45	0.095
11.84	0.156	8.48	0.190
11.88	0.234	8.52	0.285
11.88	0.312	8.55	0.380
11.96	0.390	8.59	0.475
11.99	0.468	8.64	0.570
12.06	0.546	8.73	0.665
12.14	0.624	8.90	0.760
12.30	0.702	9.54	0.856
12.70	0.780	13.53	0.951
13.87	0.869	20.22	1.000
19.38	0.938		
28.13	1.000		

Adsorption Gas Concentration <u>2999</u> PPM		Adsorption Gas Concentration <u>4998</u> PPM	
Temperature 40°C		Temperature 40°C	
Time/unit wt., min/gm	c/c ₀	Time/unit wt., min/gm	c/c ₀
4.46	0.000	4.02	0.000
4.59	0.073	4.07	0.087
4.64	0.147	4.09	0.177
4.68	0.220	4.11	0.266
4.73	0.293	4.12	0.355
4.76	0.367	4.14	0.443
4.79	0.440	4.15	0.532
4.83	0.513	4.18	0.621
4.86	0.587	4.23	0.709
4.89	0.660	4.34	0.798
4.96	0.733	4.74	0.887
5.09	0.806	6.50	0.976
5.49	0.880	9.69	1.000
7.50	0.953		
17.66	1.000		

Adsorption Gas Concentration <u>7226</u> PPM		Adsorption Gas Concentration <u>9704</u> PPM	
Temperature 40°C		Temperature 40°C	
Time/unit wt., min/gm	c/c ₀	Time/unit wt., min/gm	c/c ₀
2.61	0.000	2.29	0.000
2.64	0.056	2.32	0.084
2.66	0.111	2.33	0.169
2.67	0.167	2.34	0.253
2.69	0.272	2.34	0.337
2.71	0.278	2.35	0.422
2.73	0.333	2.36	0.506
2.74	0.389	2.37	0.590
2.76	0.444	2.38	0.675
2.77	0.500	2.42	0.759
2.78	0.556	2.53	0.843
2.79	0.611	2.97	0.926
2.81	0.667	6.44	1.000
2.83	0.722		
2.87	0.778		
2.89	0.833		
3.17	0.889		
3.76	0.944		
7.50	1.000		

APPENDIX B
SAMPLE CALCULATIONS

I. Void fraction

$$\text{Bed height (Z)} = 17.88 \text{ cm}$$

$$\text{Bed radius (R)} = 0.5461 \text{ cm}$$

$$\text{Particle density } (\rho_p) = 1.58 \text{ gm/cm}^3$$

$$\text{Weight of the bed (W)} = 14.0 \text{ gm}$$

$$\text{Bed volume (V}_B) = \pi R^2 Z = 16.748 \text{ cm}^3$$

$$\text{Particle volume (V}_p) = W/\rho_p = \frac{14.0}{1.58} = 8.8608 \text{ cm}^3$$

$$\text{Void fraction } (\epsilon) = (V_B - V_p)/V_B$$

$$\epsilon = (16.6581 - 8.8608)/16.6581$$

$$\epsilon = 0.4681$$

$$m = \frac{\epsilon}{1-\epsilon}$$

$$= \frac{0.4681}{1-0.4681} = 0.88$$

II. Equilibrium uptake

The equilibrium uptake is calculated based on the area above the breakthrough curve, which was measured by a planimeter, and the inlet concentration of the adsorbent.

$$\text{flow rate} = 62 \text{ cc/min}$$

$$\text{area} = 250.43 \text{ in}^2$$

$$T = 40^\circ\text{C}$$

$$\text{Weight of solids} = 16.0 \text{ gm}$$

$$C_0 = 9.704 \text{ PPM SO}_2 \text{ in N}_2$$

$$\text{Calibration} = 5.93 \text{ in}$$

$$\text{uptake} = \frac{9.704}{10^6} \times 62 \times \frac{250.43}{16} \times \frac{1}{5.93} = 1.5880 \frac{\text{cm}^3 \text{SO}_2}{\text{gm solid}}$$

III. Equilibrium isotherms

a. Langmuir isotherm:

The equilibrium data was fitted to the Langmuir equation using the following relation,

$$1/q^* = 1/a_1 C^* + \frac{a_2}{a_1}$$

The least square fit to find the equation representing the straight line was carried using

$$\text{slope} = \frac{\sum xy - \frac{\sum x \sum y}{n}}{\sum x^2 - \frac{(\sum x)^2}{n}}$$

$$\text{intercept} = \bar{y} - \text{slop} * \bar{x}$$

$$\text{where } \bar{y} = \sum y/n, \quad \bar{x} = \sum x/n$$

Using the equilibrium data in correct units, one would be able to find one equation representing the straight line as follows:

$$T = 10^\circ\text{C}$$

$$\begin{aligned} 1/X_1 &= 993 \text{ PPM} \times 1/10^6 \text{ cm}^3/\text{PPM} \times 2.202 \text{ mg}/\text{cm}^3 \\ &= 2.1867 \times 10^{-6} \text{ gm SO}_2/\text{cm}^3 \text{ gas} \end{aligned}$$

$$\therefore X_1 = 457334 \text{ cm}^3 \text{ gas}/\text{gm SO}_2$$

$$\begin{aligned} 1/Y_1 &= 0.8765 \times 2.202 \times 1.58 \text{ gm solid}/\text{cm}^3 \text{ solid} \\ &= 3.0496 \times 10^{-3} \text{ gm SO}_2/\text{cm}^3 \text{ solid} \end{aligned}$$

$$\therefore Y_1 = 327.92 \text{ cm}^3 \text{ solid}/\text{gm SO}_2$$

The same calculations should be followed for $X_2, Y_2, X_3, Y_3, X_4, Y_4, X_5, Y_5, X_6,$ and Y_6 .

$$\sum_1^6 XY = X_1Y_1 + X_2Y_2 + X_3Y_3 + X_4Y_4 + X_5Y_5$$

$$= 250033409.7$$

$$\sum x \sum y = 1127.35 * 1036450.24$$

$$= 1168442178$$

$$\sum x^2 = 2.9809139 \times 10^{11}$$

$$\therefore \text{slope} = \frac{250033409.7 - (1168442178/6)}{(2.980913 \times 10^{11}) - (1036450.24)^2/6}$$

$$= 4.644091 \times 10^{-4}$$

$$\text{intercept} = 187.89 - 80.22 = 107.668$$

$$\therefore Y = 4.6440901 \times 10^{-4} X + 107.668$$

$$\therefore \frac{1}{a_1} = \frac{1}{4.6440901 \times 10^{-4}}$$

$$a_1 = 2153.27433$$

$$\frac{a_2}{a_1} = 107.668$$

$$a_2 = 107.668 * 107.668 = 231840.103 \frac{\text{cm}^3 \text{ solid}}{\text{gm SO}_2}$$

$$\therefore q^* = \frac{2153.27433C^*}{1 + 231840.103C^*}$$

b. Freundlich isotherm:

$$T = 10^\circ\text{C}$$

$$\log q^* - \log(2.1841) = 0.3393$$

$$\log C^* = \log(993) = 2.9969$$

The other equilibrium uptake data is calculated in the same manner and the data is plotted as $\log C^*$ vs $\log q^*$. The Freundlich constants are obtained from the least square fit as follows:

$$\log q^* = \frac{1}{n} \log_{10} C^* + \log_{10} K$$

The slope of this equation equals to $\frac{1}{n}$. The equation representing this model is

$$Y = .38144219X - 0.30425480$$

$$\frac{1}{n} = .38144219$$

$$K = \frac{1}{0.30425480} = .49630105$$

c. Dubinin model

The equilibrium data is to be plotted as $[\log_{10}(\frac{P_i}{P_0})]^2$ vs $\log W$ to fit this model.

saturation pressure of SO_2 at $10^\circ\text{C} = 1846.98 \text{ mmHg}$

total pressure = 620 mm Hg

M.W. of $\text{SO}_2 = 64.0 \text{ gm SO}_2/\text{gm-mole}$

$$W = 2.0186 \times 10^{-3} \frac{\text{gm SO}_2}{\text{gm solid}} \times \frac{1}{64} \frac{\text{gm SO}_2}{\text{gm-mole}}$$

$$W = 3.151 \times 10^{-5} \text{ moles SO}_2/\text{gm solid}$$

$$\log_{10} W = 04.502$$

$$[\log_{10}(\frac{P_i}{P_0})]^2 = [\log_{10}(\frac{10^6 \times 1846.98}{620 \times 993})]^2 = 12.090$$

From the least square fit, the resulting straight line equation is

$$Y = -.0643542X - 3.6806579$$

$$B = -.0643542$$

$$\log_{10} W_0 = -3.6806579$$

$$W_0 = 2.086 \times 10^{-4} \text{ moles SO}_2/\text{gm solid}$$

d. Polanyi model:

In this model, W is plotted vs $\frac{\Delta G}{R}$. $\frac{\Delta G}{R}$ is calculated

from:

$$\frac{\Delta G}{R} = -T \ln\left(\frac{P}{P_0}\right)$$

$$\text{at } T = 10^\circ\text{C} = 285^\circ\text{K}$$

$$P_0 = 1846.98 \text{ mm Hg}$$

$$\frac{\Delta G}{R} = -283 \ln\left(\frac{10^6 \times 1846.98}{620 \times 993}\right) = -2265.80$$

The other data points are generated in the same manner.

IV. Heat of adsorption

At a selected loading (q^*), the equilibrium partial pressure is calculated from the corresponding concentration as follows:

$$P = 2.60837 \times 10^{-6} \frac{\text{gm SO}_2}{\text{cm}^3 \text{ gas}} \times \frac{1}{2.202} \frac{\text{cm}^3 \text{ SO}_2}{\text{mg SO}_2} \times \frac{1000 \text{ mg}}{\text{gm}}$$

$$\times 620 \text{ mm Hg} = 0.7344 \text{ mm Hg}$$

The data is plotted as $\ln(P)$ vs $\frac{1}{T}$, and the resulting straight line is obtained by a least square fit. The slope of this straight line provides $-\frac{\Delta H_s}{R}$, from which ΔH_s was calculated.

$$\begin{aligned} \Delta H_s &= 2475.21 \times 1.987 \text{ cal/mole} \\ &= 4918.25 \text{ cal/gm-mole} = 4.918 \text{ Kcal/mole.} \end{aligned}$$

V. Diffusion Coefficients

$$C_0 = 2,999 \text{ PPM SO}_2 \text{ in N}_2$$

$$T = 40^\circ\text{C} \quad a_1 = 2406.8665 \quad Z = 17.78 \text{ cm}$$

$$\eta \text{ as obtained from the curve fit} = 35.00$$

$$\text{flow rate} = 62 \text{ cm}^3/\text{min}$$

$$\begin{aligned} \text{cross section area} &= \frac{\pi D_i^2}{4} \\ &= \frac{\pi (.430)^2 \text{ in}^2}{4} \times (2.54)^2 \frac{\text{cm}^2}{\text{in}^2} \\ &= 0.9369 \text{ cm}^2 \end{aligned}$$

$$\epsilon = .4681, \quad m = \frac{\epsilon}{1-\epsilon} = \frac{.4681}{1-.4681} = .880$$

$$V = \frac{V}{\epsilon} = \frac{62}{0.9369 \times .4681} = 141.37 \text{ cm/min}$$

$$\begin{aligned} D &= \frac{mVR_1^2}{2a_1Z} = \frac{.88 \times 141.37 (.04024)^2}{3 \times 2406.86 \times 17.78} \times 35 \\ &= 5.491892 \times 10^{-5} \text{ cm}^2/\text{sec}. \end{aligned}$$

VI. Activation Energy

The Arrhenius coefficients, (E_a) and D_0 were evaluated from the slope and intercept of the straight line resulting from the plot of $\ln(\bar{d})$ vs $(\frac{1}{T})$. The diffusion coefficients at $T = 10^\circ\text{C}$ and 40°C were used.

$$\text{slope} = E_a = -1406.66 \text{ at } C_0 = 4,998 \text{ PPM in } N_2$$

$$\text{intercept} = \ln(D_0) = -9.5640$$

$$\therefore D_0 = e^{-9.5640} = 7.02114 \times 10^{-5} \text{ cm}^2/\text{sec}.$$

APPENDIX C
FLOW METER CALIBRATION CURVE

